PhD degree in Systems Medicine

(curriculum in Human Genetics)

European School of Molecular Medicine (SEMM),

University of Milan and University of Naples "Federico II"

Settore disciplinare: Bio/17 (Istologia)

A selective ER-phagy exerts procollagen quality control via a Calnexin-FAM134B Complex

Chiara De Leonibus

Tigem, Pozzuoli

Matricola n. R11466

Supervisor: Prof. Carmine Settembre

Internal Supervisor: Prof. Alberto Auricchio

External Supervisor: Prof. Maurizio Molinari

Anno accademico 2018-2019

Table of Contents

List of Abbreviations

AVs: Autophagic vesicles
LIR or GIM: LC3 or GABARAP interaction motif
ER: Endoplasmic reticulum
PC or PCs: Procollagen or procollagens
ERAD: ER-associated degradation
ERLAD: ER-to-lysosome associated degradation
ERES: ER exit sites
IM: Intramembrane
TM: Transmembrane
ATZ: Alpha1-antitrypsin Z
NPC1: NPC intracellular cholesterol transporter 1
COL1 and COL2: Type I and type II collagen
HSP47: Heat shock protein 47
COPII: Coat protein complex II
CANX: Calnexin
MEFs: Mouse embryonic fibroblasts
Saos2: Human osteoblasts
RCS: Rat chondrosarcoma cells
DFCP1: Double FYVE domain–containing protein 1
BafA1: Bafilomycin A1
LSDs: Lysosomal storage disorders
MPSI: Mucopolysaccharidosis type I
CLEM: Correlative light electron microscopy
SEDC: Spondyloepiphyseal Dysplasia Congenita
ATG: Autophagy-related proteins
PDI: Protein disulfide isomerase
CRT: Calreticulin
UGT1: UDP-glucose:glycoprotein glucosyltransferase
CST: Castanospermine
MS: Mass spectrometry
U2OS: Human osteosarcoma cell line
RT: Room temperature
FGF: Fibroblast growth factor
IRS1: Insulin receptor substrate 1
MO: Morpholino
CLEAR: Coordinated lysosomal expression and regulation
mTORC1: Mammalian target of rapamycin complex 1
PI3K: Phosphatidylinositol-3-kinase-related kinase (PI3K)
JNK: C-Jun N-Terminal kinase

Figures Index

Abstract

The endoplasmic reticulum (ER) is the largest cellular organelle adapting dynamically to cope with cellular stress and high demand of newly synthesized proteins. Protein misfolding eventually occurs in the ER and leads to protein aggregation and ER dysfunction. Mammals have developed evolutionary-conserved quality control mechanisms at the ER. ER-phagy is a novel identified pathway targeting ER portions via autophagy for lysosomal degradation. This process occurs through ER-phagy receptors, ER proteins that bind autophagosomal LC3 protein via a cytosolic LC3 interacting domain. However, the importance of ER-phagy in maintaining cellular homeostasis is still undiscovered. Moreover, the molecular mechanisms that regulate ER-phagy according to cellular needs are still largely unknown. Chondrocytes and osteoblasts are highly secretory cells with an abundant ER, producing predominantly procollagen (PC) molecules in the extracellular matrix during endochondral ossification. They reside in a poorly vascularized tissue as the growth plate with scarcity of nutrients, representing a good cellular model to study ER-phagy. We have characterized ER-phagy in PC producing cells, serving as a cellular pathway that selectively recognizes misfolded PC in the ER lumen. Specifically we found that the ER chaperone CALNEXIN acts as co-receptor that recognizes ER-luminal misfolded PC and interacts with the ER-phagy receptor FAM134B. In turn, FAM134B binds the autophagosome membrane-associated protein LC3 and delivers a portion of ER containing both CALNEXIN and PC to the lysosome for degradation. Moreover, we identified ER-phagy as a transcriptionally induced mechanism by induction of FAM134B expression during starvation and upon FGF signaling, a critical regulator of chondrocyte differentiation. In vivo, FAM134B knock-down in Medaka fish dampened cartilage growth and bone formation, suggesting a physiological function of ER-phagy during skeletogenesis. Taken together, these data unveil a role for FAM134B-dependent ER-phagy in maintaining cellular fitness in PC producing cells and suggest potential therapeutic approaches for the treatment of skeletal features in multiple human diseases.

Introduction

Macroautophagy (referred to as autophagy) is a catabolic process dedicated to the turnover of intracellular components through the sequestration of cytoplasmic material in double-membrane autophagic vesicles (AVs) that eventually fuse with lysosomes where cargo is degraded [1]. Proteins and organelles are selectively delivered to AVs via receptor-mediated processes. Autophagy receptors are constituted by a LC3 or GABARAP interaction motif (LIR or GIM, respectively) enabling the binding of the cargo to LC3 or GABARAP proteins, which decorate autophagosomal membranes [2, 3].

Different forms of selective autophagy exist depending on the cargo specificity mediated by different autophagy receptors. These forms of selective autophagy include for instance aggrephagy (for protein aggregates), glycophagy (for glycogen), ribophagy (for ribosomes), along many other types [4]. During the recent years, an additional important example of selective autophagy is emerging, the ER-phagy pathway, in which portions of the endoplasmic reticulum (ER) are sequestered within AVs and transported to the lysosomes for degradation.

However, given the complexity of the ER in terms of its cellular topology and functions, ER-phagy is not the only quality control mechanism operating at the ER. In the next section, the many diverse functions of the ER will be highlighted, along with the different mechanisms of quality control operating at the ER. Next, ER-phagy and its role in cargo degradation will be discussed, with a particular emphasis on the description of molecular mechanisms of procollagen (PC) degradation mediated by ER-phagy.

The endoplasmic reticulum (ER) as a cellular 'hub'

The ER is the largest organelle in the cell involved in diverse cellular functions, including calcium storage, lipid and protein biosynthesis, secretion and transport [5, 6]. It is considered as a cellular 'hub' for sorting both intracellular and extracellular proteins destined to different compartments: i.e. Golgi, plasma membrane, extracellular matrix along with many

others [7, 8]. To maintain high efficiency in all the above functions, the ER needs to dynamically adapt to handle cellular stress conditions and high demand of newly synthesized proteins [9, 10]. Importantly, errors in protein synthesis and folding eventually occur and induce protein misfolding and aggregation, thus leading to ER stress and culminating in cell death [11, 12]. The disruption of cellular fitness caused by ER stress is at the basis of multiple human disorders, including neurodegenerative diseases, being the most frequent, or ageing conditions such as late-onset type 2 diabetes, atherosclerosis and cataracts among many others [13-16]. In fact, an impairment of ER functions or inefficiency of the cellular degradative mechanisms is often associated to bacterial and viral infection or to 'conformational diseases' [13-15, 17-20], in which misfolded proteins aggregate at the ER with disruption of both cellular and tissue fitness. Notable examples are represented by Osteogenesis Imperfecta and Dysferlinopathy, which are caused by the accumulation of protein inclusions in the ER lumen (i.e. procollagen and dysferlin), in which the induction of autophagy has been shown to enhance their degradation and ameliorate cellular distress [21, 22].

Quality control mechanisms operating at the ER

Mammals have developed evolutionary-conserved and internal quality control mechanisms at the ER, by which newly synthesized proteins are 'proof-read'. This mechanism allows that only the properly folded proteins can exit from the ER and are destined to the secretory pathway [23]. The best characterized of these quality control mechanisms, is the ER-associated degradation (ERAD) pathway, a process by which folding of proteins is continuously monitored and misfolded polypeptides are dislocated from the ER to the cytosol to be degraded by the 26S proteasome [24, 25]. However, the role of additional quality control mechanisms is increasingly emerging, as not all misfolded ER clients are

eligible for ERAD, and thus must be cleared from the ER through other alternative, ERAD-independent, processes.

The lysosomal system is a main centre for cellular clearance, involved in the degradation and recycling of unwanted cytosolic material and cellular waste [26]. Up to now, an increasing list of misfolded proteins, including mutant forms of alpha1-antitrypsin, hormones or hormone receptors and proalpha1 (I) chains of type I procollagen has been shown to be excluded from the ERAD pathway [27-30]. Intracellular substrates are delivered to the lysosomes via different routes including, at least three alternative, ERAD-independent, pathways. In addition to the canonical ERAD pathway (**A**), the alternative quality control pathways include: **B**) ER-phagy (requiring macroautophagy, discussed next) [31, 32]; **C**) microautophagy [33] or **D**) ER-to-lysosome associated degradation (ERLAD) (**Figure 1**) [34]. As previously discussed, whereas in macroautophagy the cytosolic material is delivered to lysosomes via autophagosomes, in microautophagy lysosomal membranes directly engulf and sequester cytosolic targets for degradation, that include ER fragments or ER exit sites (ERES), a mechanism generally described as 'ERES-microautophagy' and it requires components of the autophagy machinery [1, 35],[36]. Conversely in the ERLAD pathway, the protein aggregates are first segregated in ER subdomains, then enclosed in single-membrane ER vesicles that eventually fuse with lysosomal degradative organelle, not requiring autophagosomes or component of the autophagy machinery [34].
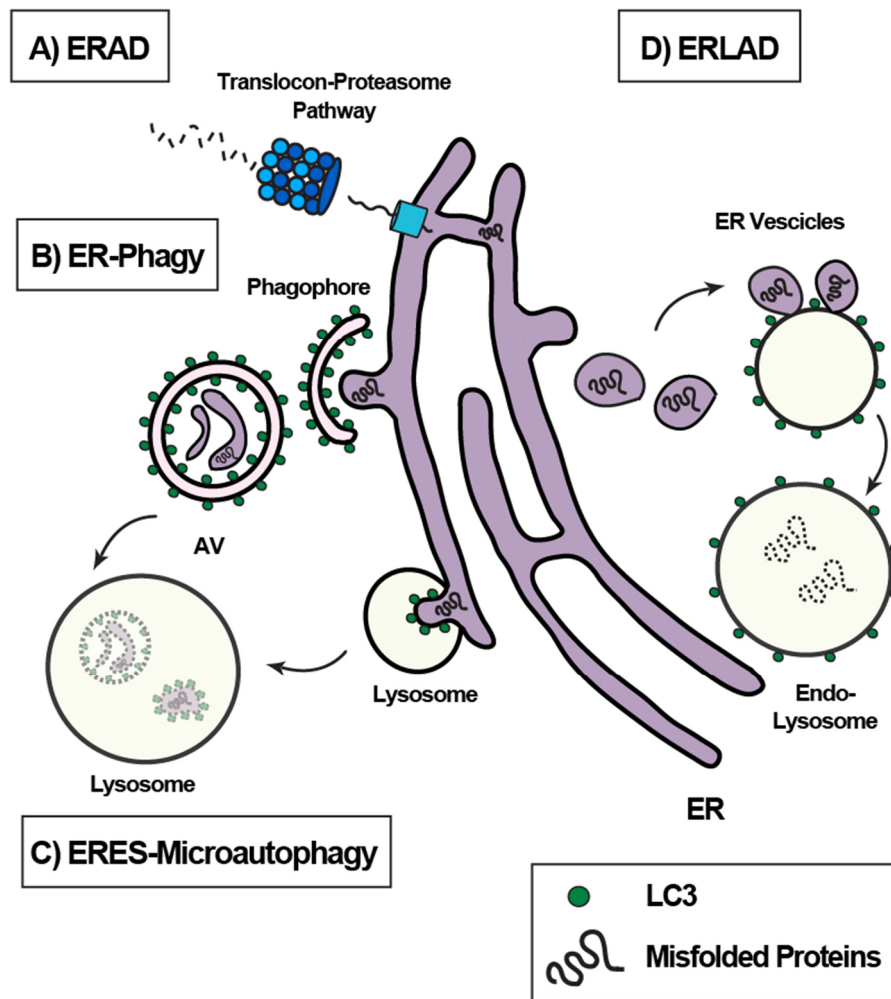
Figure 1. Quality control mechanisms of clearance operating at the endoplasmic reticulum (ER).

A) The ER associated degradation (ERAD) requires the Translocon-Proteasome complex to dislocate misfolded proteins from the ER to the cytosol and degrade them, respectively. **B)** In ER-phagy, ER fragments are sequestered by a double-membrane autophagosome decorated with LC3 molecules (green dots). Autophagosomes then fuse with lysosomes for degradation. **C)** In ERES-microautophagy, lysosomal invagination or protrusion directly engulfs portions of ER or ER exit sites (ERES) decorated with LC3 molecules (green dots). **D)** In ER-to-lysosome associated degradation (ERLAD), single membrane ER-derived vesicles bud from the ER and fuse with lysosomes for degradation. Abbreviations: ER, endoplasmic reticulum; AV, autophagic vesicle.

The 'ER-phagy' pathway, its receptors and functions

The term 'ER-phagy' was first identified in yeast for defining the process of selective clearance of the ER by the vacuoles (the yeast lysosome) exposed to cellular redox perturbations or starvation [37, 38]. Although this process was described to be autophagy-independent [39], more recently it has been shown in yeast that ER fragments can be sequestered into Atg8-positive autophagosomes upon nutrient starvation or TOR inhibition by Rapamycin [40]. A similar process has been successively described in mammalian cells that during starvation induce selective engulfment of ER fragments into autophagosomes for lysosomal degradation [41].

The ER is composed of a complex structure that forms a continuous membrane network made of cisternae (or sheets) and tubules spreading from the nucleus to the plasma membrane [42]. Cisternae and tubules are mostly connected through three-way junctions, which result in an ER having a cellular polygonal pattern [43]. However, the complexity of ER structure has been further elucidated by ultra-structural studies using super-resolution electron microscopy, having identified membrane sheets as densely packed tubular arrays, also defined as ER matrix, with a rapid dynamic reorganization to allow many cellular functions [44]. Up to now, distinct and specialized ER-phagy receptors have been identified in mammals, including SEC62, CCPG1, TEX264, FAM134B, ATL3 and RTN3 [31, 41, 45-50]. FAM134B, RTN3 and ATL3 are proteins with an intramembrane (IM) region lacking an ER luminal domain, having functions in shaping ER, modulating tubule/sheet ratio and tubule branching [51, 52]. FAM134B targets perinuclear sheets, whereas RTN3 and ATL3 target ER tubules. On the contrary, CCPG1, SEC62 and TEX264 are transmembrane (TM) proteins with a cytosolic, ER-membrane and ER-luminal domains with no reported function in shaping ER membranes. Although transmembrane receptors are ubiquitous in the ER, TEX264 has been recently observed at three-way junctions suggesting that it might be enriched in these subdomains [53]. Notably, SEC62 is a constituent of the translocon

complex regulating protein import in the mammalian ER. All ER-phagy receptors share one or more LC3 interaction motif (LIR) that facilitates binding of the cargo to LC3 proteins, which decorate autophagosomal membrane, thus leading the delivery of ER fragments to autophagosomes (**Figure 2, Table 1**) [2].

ER-phagy is implicated in a variety of cellular functions having fundamental cytoprotective roles. In fact, it is involved in re-shaping ER after expansion under cellular stress and protein synthesis overload, as described in B and T lymphocytes [54, 55]. SEC62-mediated ER-phagy promotes recovery from ER stress, in a series of events called RecovER-phagy. In this process, ER portions are selectively cleared in order to re-establish ER homeostasis and chaperone content [45]. However, ER-phagy is also implicated in removing misfolded cargoes from the ER and controlling cellular proteostasis, a cellular process discussed next.
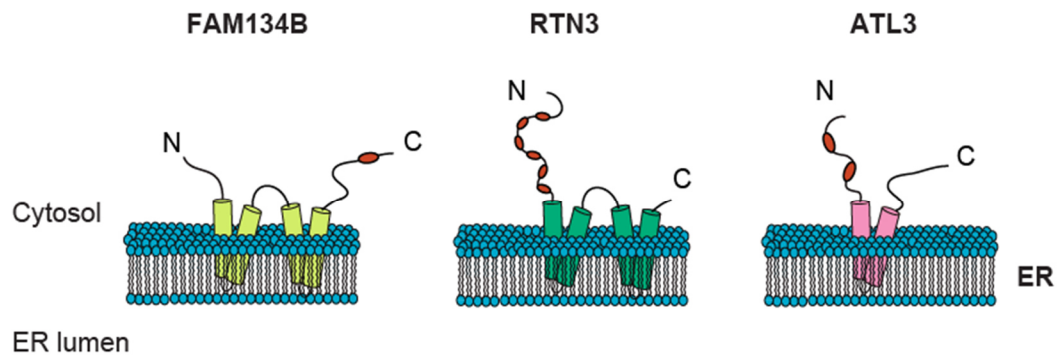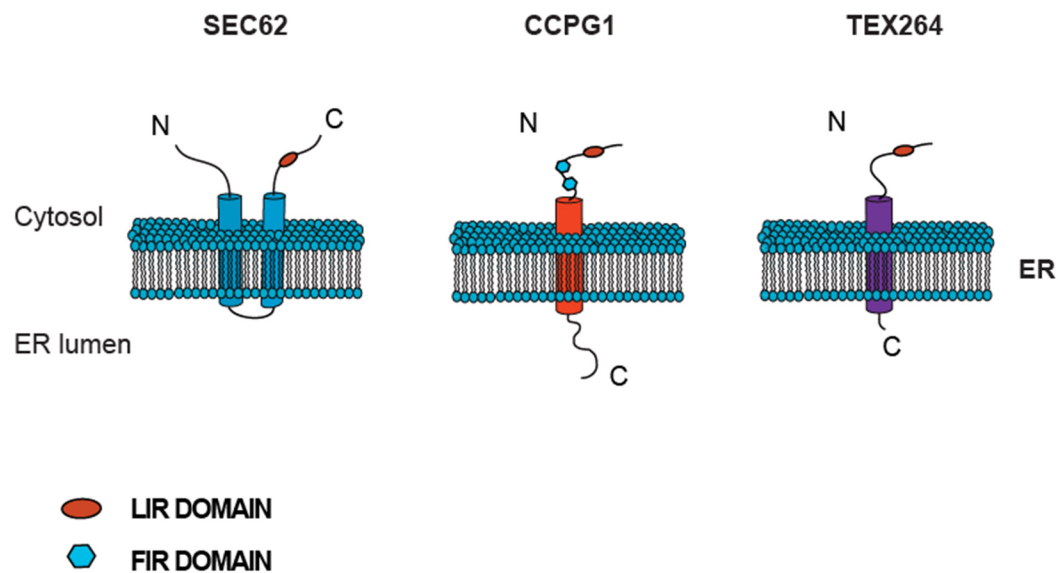
Figure 2. The ER-phagy receptors in mammals.

The upper panel shows intramembrane receptors: FAM134B, RTN3 and ATL3 that are proteins with an intramembrane region lacking an ER luminal domain. The lower panel shows transmembrane receptors: SEC62, CCPG1 and TEX264 with a cytosolic, ER-membrane and ER-luminal domains. All ER-phagy receptors share one or more LC3 interaction region (LIR). CCPG1 also contains two FIP200 interaction regions (FIR). Abbreviations: ER, endoplasmic reticulum; N, N-terminal domain; C, C-terminal domain; LIR, LC3 interaction region; FIR, FIP200 interaction region.

Table 1. Mammalian ER-phagy receptors and their general characteristics.

Structure	Receptor	Domains (LIR domain common to all)	Process involvement at the ER
IM	FAM134B	Intramembrane Reticulon-Homology Domain (RHD)	ER-phagy ERLAD
	RTN3	Intramembrane Reticulon-Homology Domain (RHD)	ER-phagy
	ATL3	Intramembrane Dynamin-like GTPase Domain	ER-phagy
TM	CCPG1	FIP200-interacting region (FIR domain)	ER-phagy
	SEC62		RecovER-phagy
	TEX264		ER-phagy

Abbreviations: IM, Intramembrane; TM, Transmembrane.

The ER-phagy serves in the selective-mediated degradation of ER misfolded cargoes

Another emerging function of ER-phagy is the degradation of ER portions containing misfolded protein clients as a back-up or alternative pathway to ERAD. The *in vivo* deletion of CCPG1 in mice is associated to the accumulation of ER insoluble proteins in exocrine pancreatic cells [31], thus highlighting the physiological importance of ER-phagy in removing aberrant protein products from the ER lumen. Moreover, the identification of multiple ER-phagy receptors suggests that different ER cargos might be subject to different types of ER-phagy.

Up to now, FAM134B and RTN3 have emerged as the major ER-phagy receptors to have a fundamental role in the selective removal of specific cargoes, including *i)* for FAM134B, mutant forms of alpha1-antitrypsin Z (ATZ) and NPC Intracellular Cholesterol Transporter 1 (NPC1) or *ii)* for RTN3, mutant type of proinsulin (*Akita* mutant) [34, 56, 57].

Procollagen-selective clearance mediated by ER-phagy

Collagens represent the most abundant molecules among the ER proteins. Type I and type II collagen (COL1 and COL2) are the major protein components of bone and cartilage,

respectively [58]. The biosynthesis of procollagen occurs in multiple steps, summarized in **Figure 3**.

Procollagens (PCs) are synthesized as alpha I and alpha II chains and folded into triple helices of procollagen in the ER [58]. Properly folded PCs associate with the Heat Shock Protein 47 (HSP47) chaperone and then leave the ER through ERES sub-regions, within coat protein complex II (COPII) coated carriers, and move along the secretory pathway [59]. Previous studies demonstrated that approximately 20% of newly synthesized type I procollagen (PC1) is degraded by lysosomes as a consequence of inefficient PC1 folding or secretion; this fraction significantly increases in cases of PC1 mutations [27, 60]. Similar data have been observed *in vivo*, in which a fraction of type II procollagen (PC2) produced by chondrocytes of the growth plate is degraded by autophagy [61-63]. The inactivation of autophagy pathway results in PC2 accumulation in the ER and defective formation of the extracellular matrix [61, 63]. Overall, these data clearly indicate that aberrant PC molecules represent ERAD-resistant substrates where autophagic clearance emerges as a crucial and physiologically relevant event in the maintenance of cellular and organ homeostasis. However, to date, the mechanism by which misfolded ER luminal PC is recognized by the cytosolic autophagic machinery and delivered to the lysosomes remains to be understood.

In this study, we sought to uncover the mechanisms that select non-native PC in the ER lumen for lysosomal delivery and clearance. We found that the misfolded PC molecules (e.g. HSP47 negative) are cleared from the ER through FAM134B-mediated ER-phagy. Notably, FAM134B binds PC molecules in the ER through the interaction with the transmembrane ER chaperone CALNEXIN (CANX) that acts as a specific FAM134B ER-phagy co-receptor for misfolded PCs. The formation of this complex allows the selective delivery of PC molecules to the lysosomes for degradation.
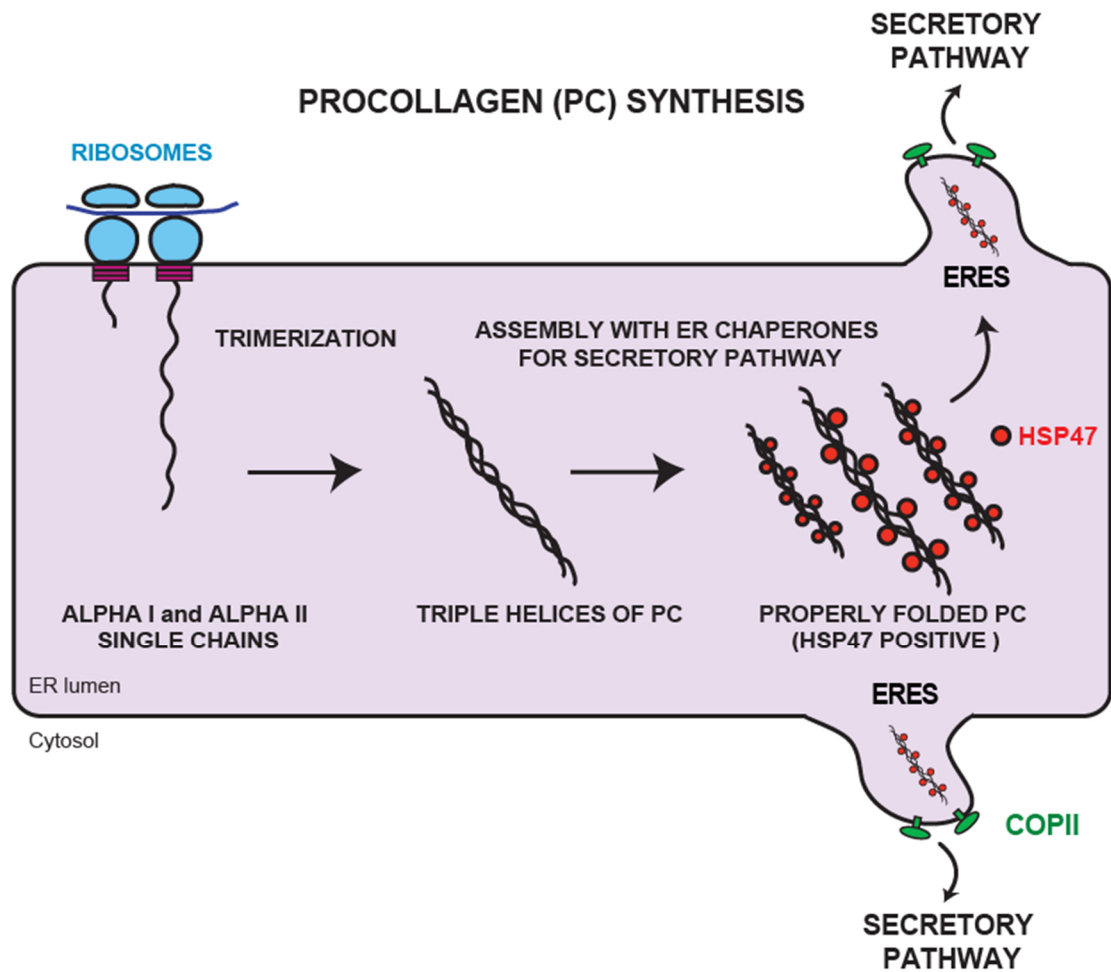
Figure 3. Steps for procollagen (PC) synthesis.

Procollagen synthesis requires multiple steps: *i)* It is synthesized as alpha I and alpha II single chains by ribosomes. *ii)* It is folded into triple helices of procollagen (PC). *iii)* The properly folded PC associates with the Heat Shock Protein 47 (HSP47) chaperone. *iv)* PC molecules then leave the ER through ERES sub-regions, within coat protein complex II (COPII) coated carriers, and move along the secretory pathway. Abbreviations: ER, endoplasmic reticulum; PC, procollagen; ERES, ER-exit sites; COPII, coat protein complex II; HSP47, Heat Shock Protein 47 chaperone.

Results

Autophagy promotes degradation of intracellular PCs

Using three collagen producing cell lines, such as mouse embryonic fibroblasts (MEFs), human osteoblasts (Saos2) and rat chondrosarcoma cells (RCS), stably expressing the autophagosome membrane marker LC3 fused with GFP (GFP-LC3), we observed co-localization of LC3 positive vesicles (hereafter referred as autophagic vesicles, AVs) with PC1 (MEFs and Saos2) and PC2 (RCS) (**Figure 4**).
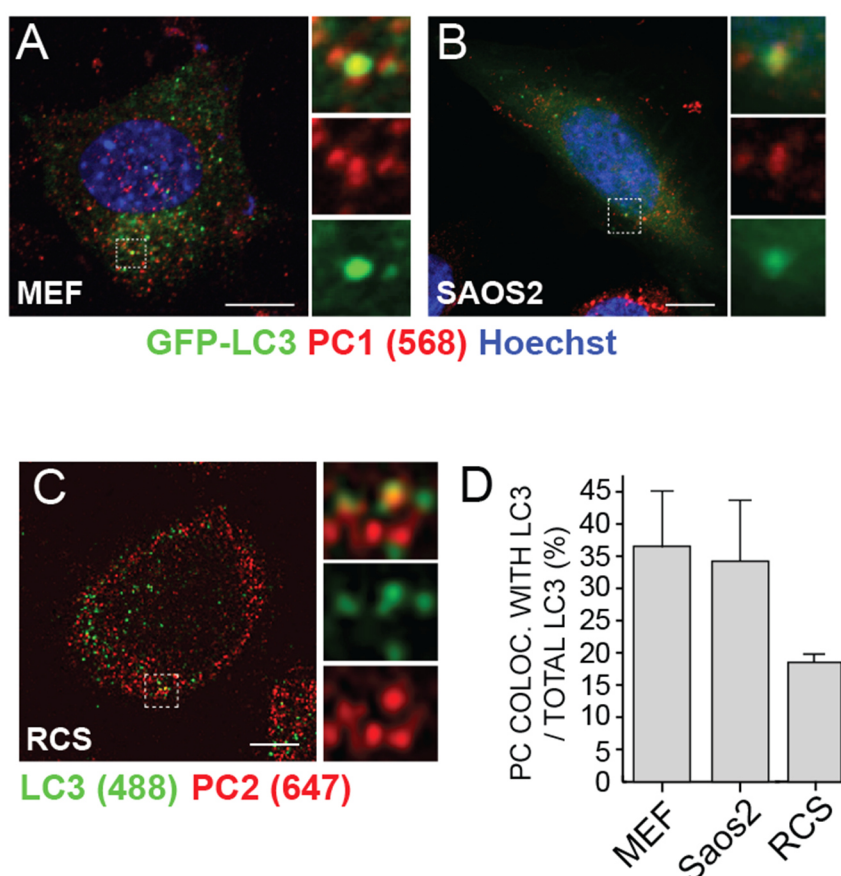
Figure 4. Procollagen is an autophagy substrate.

(**A, B**) Airyscan confocal analysis of PC1 colocalization with GFP-LC3 in (**A**) MEF (**B**) Saos2. Scale bars = 10 μm. (**C**) Airyscan confocal analysis of PC2 colocalization with LC3 in RCS cells. Scale bars = 10 μm. (**D**) Quantification of GFP vesicles positive for PC1 or PC2, expressed as % of total LC3 (mean +/- SEM), n = 18 cells (MEFs and Saos2); n=12 (RCS) from 3 independent experiments.

Similarly, we observed the colocalization of PC1 spots with the GFP-tagged double FYVE domain–containing protein 1 (DFCP1), which labels sites for autophagosome biogenesis (omegasomes) (**Figure 5, A-B**). *In vivo*, osteoblasts of the mandible in Medaka fish embryos (stage 40), showed the presence of AVs containing PC1 molecules (**Figure 5, C-E**).
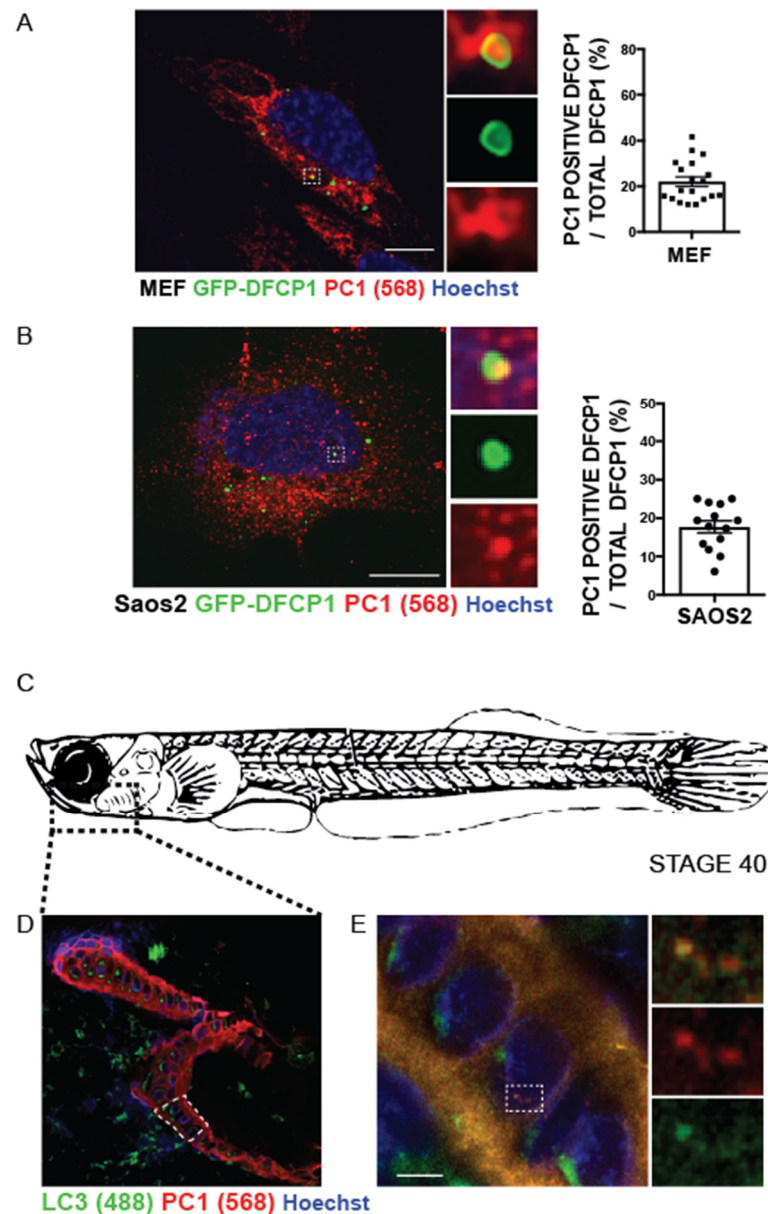
Figure 5. PC1 is an autophagy substrate.

(**A, B**) Representative immunofluorescence in (**A**) MEF and (**B**) Saos2 and quantification of AVs positive for GFP-DFCP1 containing PC1 expressed as % of total DFCP1 per cell (mean +/- SEM). Scale bar = 10 μm. (**A**) n=19 and (**B**) n=14 cells counted per condition. N=3 independent experiments. (**C**) Schematic representation of a stage 40 medaka fish. Dotted box represents area of mandible shown in (**D** and **E**). (**D**) Scanning confocal image of mandible from stage 40 medaka, immunostained with LC3 (488, green), PC1 (568, red) and

19

nuclei stained with Hoechst (blue). Dotted box represents area of mandible containing osteoblasts that was further analysed in (**E**). Scale bar = 20 μm. (**E**) Airyscan confocal image of mandible at higher magnification, scale bar = 3 μm. Boxes on the right show magnification of boxed area.

PCs accumulate and are degraded in the lysosomes

When MEFs, Saos2 and RCS cells were treated with the lysosomal inhibitor Bafilomycin A1 (BafA1), PC accumulated in the lumen of swollen endo/lysosomes (LAMP1 positive organelles, hereafter referred as lysosomes) (**Figure 6A**). Western blot analysis confirmed the accumulation of intracellular PCs, as well as of the autophagy markers LC3-II and SQSTM1, in cells treated with BafA1 compared to untreated cells (**Figure 6B**). BafA1 wash-out induced a rapid clearance of PC1 and PC2 from lysosomes of MEFs and RCS, respectively, in line with the notion that PCs are degraded in this compartment (**Figure 6C**).
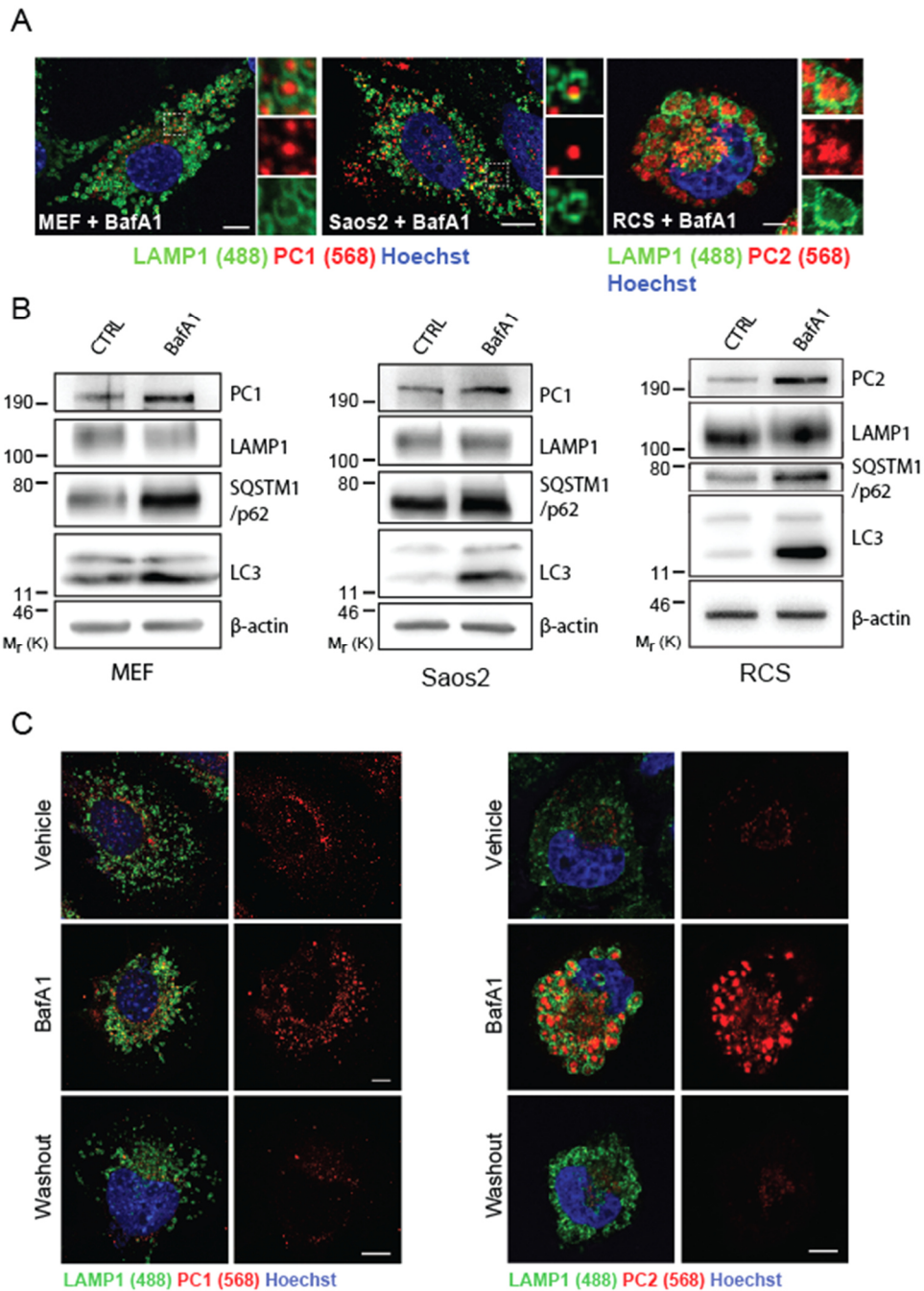
Figure 6. PCs accumulate and are degraded in the lysosomes.

(**A**) Scanning confocal microscopy analysis of MEFs, Saos2 and RCS cells treated with BafA1, immunolabeled for PC1 or PC2 (568, red) and LAMP1 (488, green). Nuclei were stained with Hoechst (blue). Scale bars = 10 μm. (**B**) MEFs, Saos2 and RCS were untreated or treated with 100nM BafA1 for 6h in MEFs, 100nM BafA1 for 9h in Saos2, 200nM BafA1 for 6h in RCS, then lysed and analysed by western blot. Bands were visualised with antibodies against PC1, PC2, LAMP1, SQSTM1/p62, LC3 and β-ACTIN. Western blots are representative of 3 independent experiments. (**B, C**) (**B**) MEFs or (**C**) RCS treated with vehicle, 100 nM BafA1 for 4 h, followed by 4h washout. Cells immunolabeled with LAMP1 (488, green) and PC1 or PC2 (568, red). Nuclei were stained with Hoechst (blue). Scale bars = 10 μm.

Lysosomal storage disorders (LSDs) represent genetic diseases characterized by an altered lysosomal degradative capacity due to mutations in genes encoding for lysosomal proteins. As a result, lysosomal substrates progressively accumulate within the lumen of lysosomes causing lysosomal swelling and cell dysfunction. We determined whether PC molecules accumulated in the lysosomes of LSD osteoblasts. Saos2 osteoblasts in which the alpha-L-iduronidase gene was deleted using CRISPR-Cas9 technology (CRISPR-IDUA) represent a disease model of mucopolysaccharidosis type I (MPS I), a lysosomal storage disorder with severe skeletal manifestations [64]. Similarly, to cells treated with BafA1, CRISPR-IDUA showed swollen lysosomes, suggesting an accumulation of undigested substrates in the lysosomal lumen. Moreover, the level of PC1 in lysosomes, and in the whole cell lysate, was higher in CRISPR-IDUA Saos2 compared to control cells (**Figure 7**).
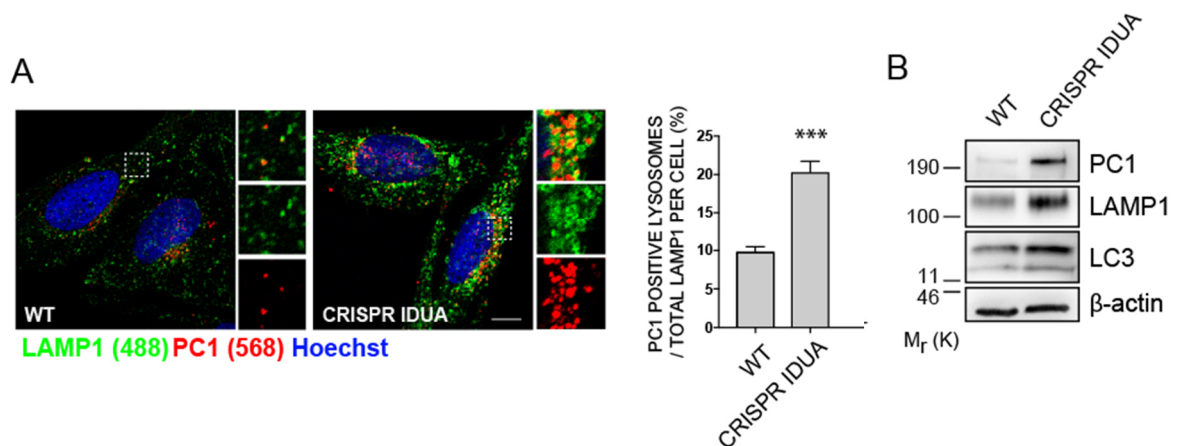
Figure 7. PCs accumulate in CRISPR-CAs9 IDUA Saos2 as a prototype of LSD.
(**A**) Scanning confocal microscopy analysis of Saos2 WT and CRISPR-Cas9 *IDUA* Saos2 at steady state, immunolabeled for PC1 (568, red) and LAMP1 (488, green). Nuclei were stained with Hoechst (blue). Scale bar = 10 μm. Bar graph shows quantification of lysosomes containing PC1 expressed as % of total LAMP1 per cell (mean +/- SEM). n= 31 cells counted per condition; 3 independent experiments. Student's unpaired, two-tailed T-Test *** P<0.0001. (**B**) WT and CRISPR *IDUA* Saos2 lysed and analysed by western blot. Bands were visualised with antibodies against PC1, LAMP1, LC3 and β-ACTIN. Data are representative of 3 independent experiments.

Autophagy sequesters PC molecules in the ER

A temperature shift assay was performed in order to understand at which trafficking stage PC became an autophagy substrate. In this assay, PC accumulates in the ER during incubation at 40 °C, and is released from the ER upon shift of the temperature to 32 °C. U2OS cells expressing GFP-LC3, mCherry-PC2 and ER marker RDEL-HALO, were imaged upon shift to 32 °C (time 0 sec). We observed that PC2 spots formed at the ER and progressively accumulated GFP-LC3 (**Figure 8A**).

We also performed Correlative Light Electron Microscopy (CLEM) and electron tomography on GFP-LC3 expressing Saos2 cells, showing that PC1 and CANX are found together in a small vesicle contained within a larger LC3-positive vesicle (**Figure 8B**). Taken together these data suggest that PC molecules are sequestered within LC3-positive vesicles when they are still within the ER.
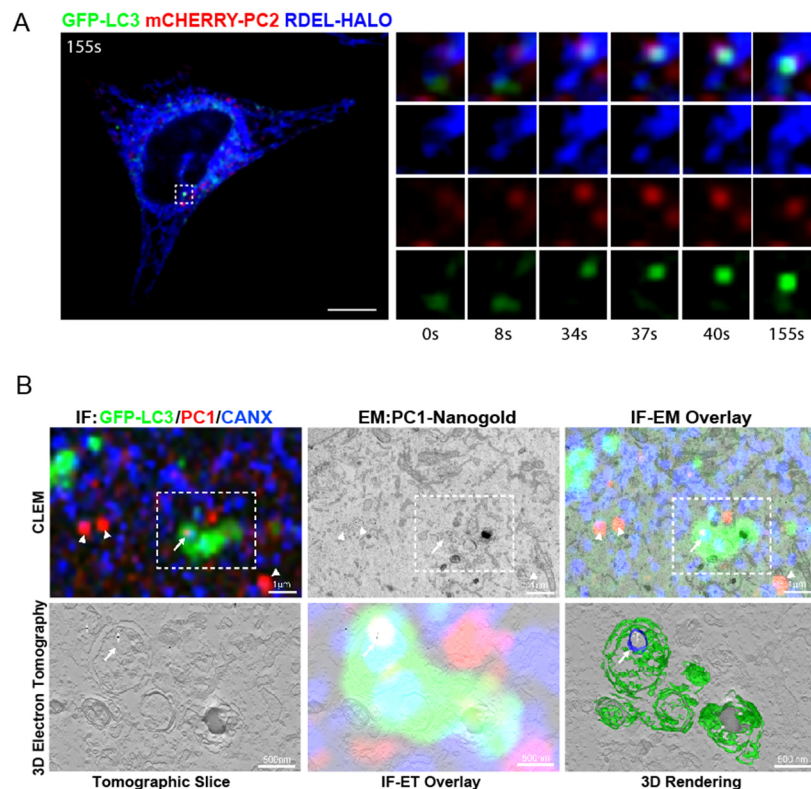
Figure 8. Autophagy sequesters PC molecules in the ER.
(**A**) U2OS expressing GFP-LC3 (green), mCherry-PC2 (red) and RDEL-HALO (blue) were imaged live by spinning disc microscopy. Single and merge channels time-lapse stills from the boxed region are shown on the right. Scale bar = 10 µm. (**B**) Correlative Light Electron

Microscopy (CLEM) and Electron Tomography of Saos2 cells transfected with GFP-LC3 (green) and labelled for PC1 (568, red and nanogold particles) and CANX (647, blue). Cells were first imaged by confocal microscopy (top left panel) and then the same region was retraced in EM (upper middle panel) and overlay is shown (upper right panel). Arrow indicates a LC3 positive vesicle containing CANX and PC1 molecules. Single tomography slice (left panel), overlay with immunofluorescence (IF) (central panel) and IF 3D rendering of AV (green) and the CANX positive vesicle containing gold particles of labelled collagen (blue and white respectively) inside an AV (right panel).

Mutant Procollagens are targeted to the lysosome at higher rates compared to WT

The collagen-specific chaperone HSP47 was excluded from the AVs containing PC1 in MEFs (**Figure 9**, **A-B**), strongly suggesting that the autophagy sequesters non-native PC1 molecules in the ER, in line with previous results [21, 61]. To further confirm this notion in a disease condition, we investigated two missense mutations in the COL2a1 protein (R789C and G1152D) that induce misfolding of the PC2 triple helix and accumulation within the ER of chondrocytes with dilated ER sheets [65]. The mutations cause a type II collagenopathy in humans, named Spondyloepiphyseal Dysplasia Congenita (SEDC) [66]. When expressed in chondrocytes the R789C- and G1152D- mutants were targeted to the lysosomes at higher rates compared with WT COL2. Notably, pharmacological enhancement of autophagy with the autophagy inducing peptide Tat-BECLIN-1 [67] increased targeting of WT and of mutant PC2 molecules to lysosomes. Opposite results were observed by treating cells with the autophagy inhibitor SAR405 (**Figure 9C**). Taken together these data suggest that autophagy preferentially degrades non-native misfolded PC molecules, preventing their accumulation in the ER.
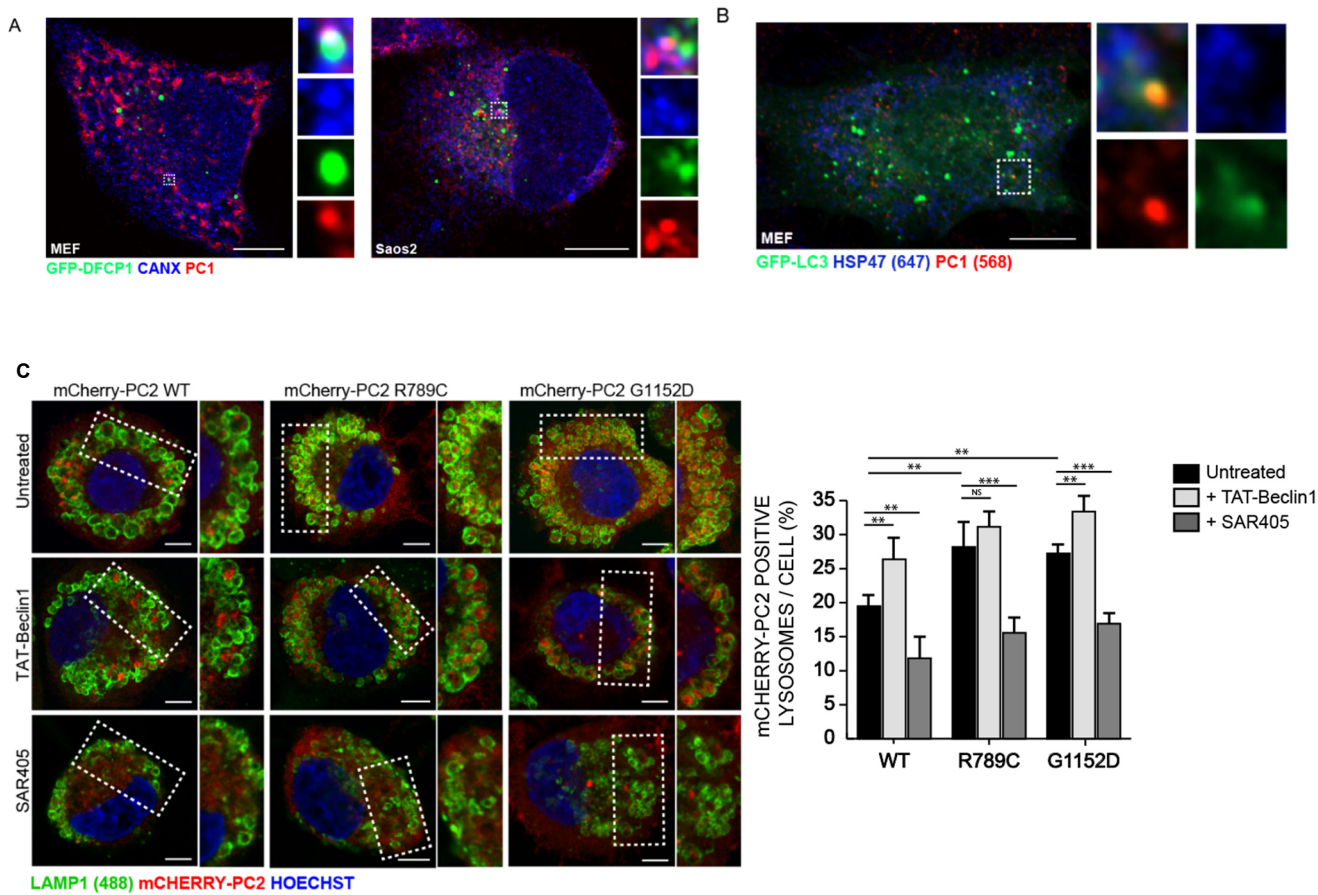
Figure 9. Misfolded PC in the ER is targeted to lysosomes via autophagy.

(**A**) DFCP1, a marker of autophagosome biogenesis co-localizes with PC1 and CANX. GFP-DFCP1 (green) expressing MEF and Saos2 immunolabelled for PC1 (568, red) and CANX (647, blue). Scale bars = 10 μm. (**B**) HSP47 is excluded from PC1 containing autophagosomes. GFP-LC3 (green) expressing MEFs immunolabelled for PC1 (568, red) and HSP47 (647, blue). Scale bars = 10 μm. (**C**) RCS cells were transiently transfected with mCherry-PC2 WT, R789C or G1152D mutants (568, red) and treated for 6h with 100nM BafA1, and as indicated with SAR405 or Tat-BECLIN-1. Cells were fixed and immunolabelled for LAMP1 (488, green). Nuclei were stained with Hoechst (blue). Scale bars = 10 μm. Bar graph shows quantification of LAMP1 vesicles positive for mcherry-PC2, expressed as % of total lysosomes per cell (mean +/- SEM), minimum of n=11 cells per genotype. Two-way ANOVA with TUKEY's post-hoc test performed and P value adjusted for multiple comparisons. ** $P<0.005$; *** $P<0.0001$.

FAM134B is required for autophagy of procollagen

Different autophagy-related (ATG) proteins and receptors are involved in autophagosome formation and cargo recognition, respectively [68].

To characterize the autophagy machinery that enables the delivery of PC molecules to lysosomes, we silenced genes belonging to different functional autophagy clusters in Saos2 cells treated with BafA1, and quantified the efficiency of PC1 delivery to the lysosomes. As expected, we found that the silencing of all genes tested involved in AV biogenesis significantly inhibited the delivery of PC1 to the lysosomes.

Notably, among autophagy and ER-phagy receptors, we found that *FAM134B* silencing most effectively inhibited PC1 delivery to lysosomes (**Figure 10A**). Our siRNA data was further validated using MEFs knocked-out for genes involved in AV biogenesis, namely *Fip200* (*Fip200$^{-/-}$*), *Atg7* (*Atg7$^{-/-}$*) or *Atg16l* (*Atg16l$^{-/-}$*) as well as in MEFs lacking *Fam134b* expression (CRISPR *Fam134b*). The effect of *Fam134b* knockout was specific, since MEFs lacking *Sec62* expression (CRISPR *Sec62*), a different ER-phagy receptor [45], showed a normal rate of PC1 delivery to the lysosomes (**Figure 10B-D**).
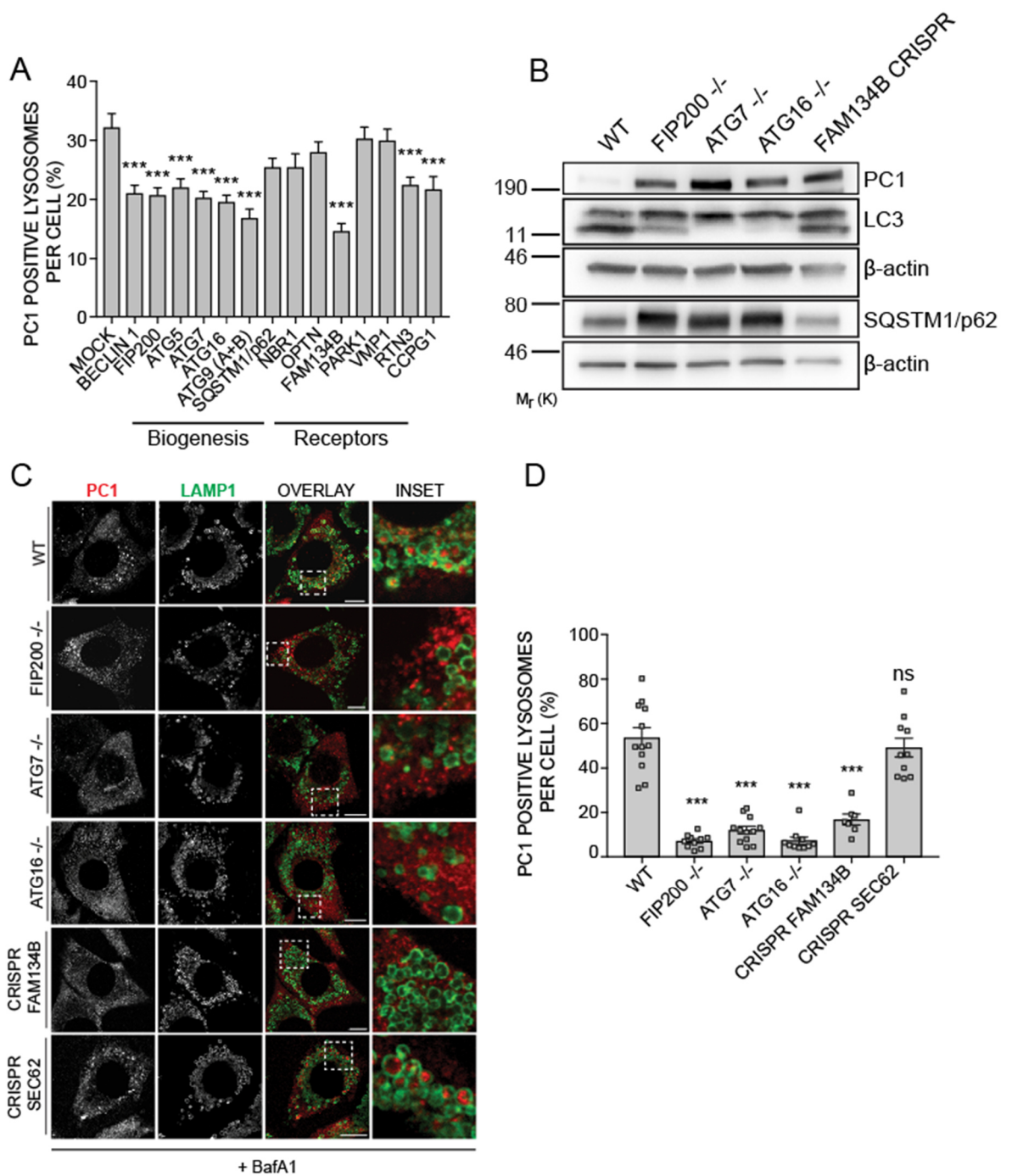
Figure 10. FAM134B is required for autophagy recognition of PC1.

(**A**). Bar graph shows quantification of lysosomes (LAMP1$^+$) containing PC1 expressed as % of lysosomes (mean +/- SEM) in Saos2 cells mock transfected or transfected with SiRNA against the indicated genes, treated with 100 nM BafA1 for 9h. n=20 cells per condition; three independent experiments. One-way ANOVA (P<0.0001) with Dunnett's multiple comparisons test performed, ***P<0.0001. (**B**) WT and KO MEFs for indicated genes were lysed at steady state and analysed by western blotting. Bands were visualised with antibodies against PC1, SQSTM1/P62, LC3, β-Actin as controls. Western blots are representative of 3 independent experiments. (**C**) MEF cell lines knock-out or CRIPSR-Cas9 for indicated

genes were treated for 12h with 50 nM BafA1, fixed and immunolabeled for PC1 (red, 568) and LAMP1 (green, 488). Scale bar = 10 μm. Insets show magnification of the boxed area. (**D**) Bar graph shows quantification of LAMP1 vesicles positive for PC1, expressed as % of total lysosomes (mean +/- SEM), n=12, 10, 12, 10, 7, 10 cells per genotype respectively; 3 independent experiments. One-way ANOVA with Dunnett's multiple comparisons test performed and P value adjusted for multiple comparisons. *** P<0.0001.

PC is the main substrate to accumulate in CRISPR Fam134b MEFs

Western blot and immunofluorescence analyses confirmed the accumulation of intracellular PC1 in CRISPR *Fam134b* MEFs compared to control cells. Notably, there was not a generalized accumulation of other ER proteins (VAPA, SEC23A and the soluble ER chaperone Protein Disulfide Isomerase [PDI]) (**Figure 11A-C**).

The impaired delivery of PC1 to lysosomes in CRISPR *Fam134b* MEFs was rescued by reintroducing WT human FAM134B, but not a FAM134B protein lacking the (LIR) motif (FAM134Blir), in which interaction with LC3 is abolished [41] (**Figure 11D**). Taken together these data strongly suggest a primary role of FAM134B in mediating the delivery of ER resident PC molecules to lysosomes.
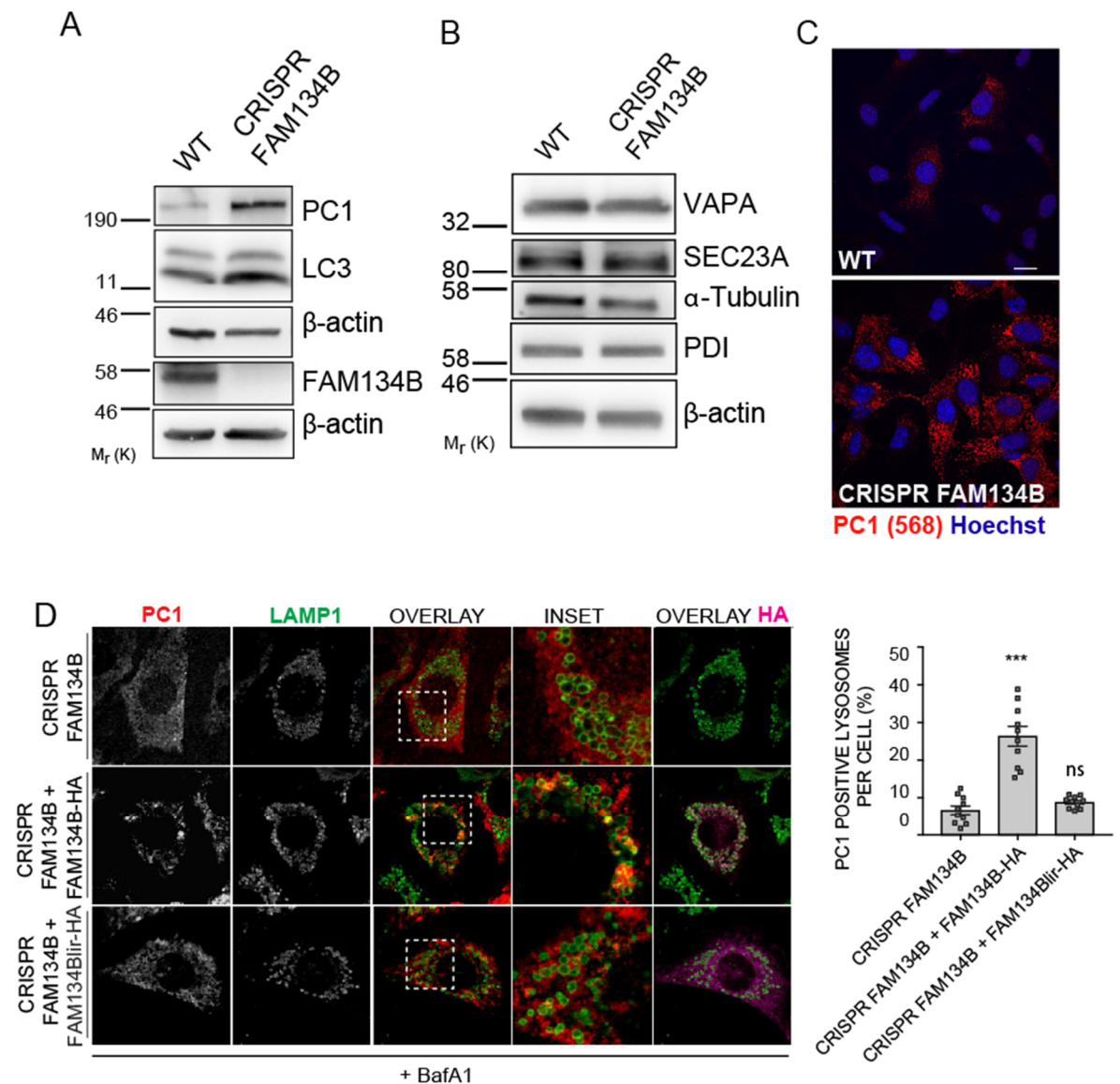
Figure 11. FAM134B absence causes specific intracellular accumulation of PC1 and fails to increase accumulation of other ER resident proteins.

(**A**) WT and CRISPR-Cas9 *Fam134b* knockout MEFs were treated as indicated, lysed and analysed by western blot. Bands were visualised with antibodies against PC1, LC3 and FAM134B. β-actin was used as a control. Western blots are representative of 4 independent experiments. (**B**) WT and KO MEFs for indicated genes were lysed at steady state and analysed by western blotting. Bands were visualised with antibodies against VAPA, SEC23A and PDI. α-tubulin or β-actin were used as controls. Western blots are representative of 3 independent experiments. (**C**) WT and CRISPR-Cas9 *Fam134b* MEFs were immunolabeled for PC1 (568, red), nuclei stained with Hoechst (blue) and analysed by scanning confocal microscopy, scale bar = 10 μm. (**D**) CRISPR-Cas9 *Fam134b* knockout MEF mock transfected or transfected with wild type FAM134B-HA or FAM134Blir-HA. Cells were treated for 12h with 50 nM BafA1, immunolabeled for PC1 (568, red), LAMP1

(488, green) and HA (647, violet) and analysed by scanning confocal microscopy. Scale bar = 10 μm. Inset panels shows magnification of the boxed area. Bar graph shows quantification of LAMP1 vesicles positive for PC1, expressed as % of total lysosomes (mean +/- SEM), quantification of n=10 cells per treatment; 3 independent experiments. One-way ANOVA with Dunnett's multiple comparisons test was performed *** P<0.0001.

CALNEXIN is required for autophagy of procollagen

FAM134B is not predicted to have an ER luminal domain, so is unlikely a direct interaction with PC molecules in the ER. We also hypothesized that the PC molecules destined for degradation need to be selectively recognized by ER quality control machinery in order to be subjected to FAM134B-mediated ER-phagy. Therefore, we investigated the involvement of ER chaperones in autophagy of PC. Taking advantage of a published list of putative PC1 and FAM134B ER interactors [46, 69], we silenced different ER genes by RNAi. The silencing of the transmembrane chaperone CANX most effectively inhibited the delivery of PC1 to lysosomes in Saos2 cells treated with BafA1 (**Figure 12A**). Similar to what we observed in CRISPR *Fam134b* MEFs, $Canx^{-/-}$ MEFs showed an accumulation of intracellular PC1 but not of other ER-resident proteins (VAPA, SEC23A and PDI) (**Figure 12B-C**). When WT MEFs were treated with BafA1, the intracellular PC levels increased as consequence of defective lysosomal degradation. Conversely, in $Canx^{-/-}$ MEFs no further increase was observed in presence of BafA1, implying that no lysosomal accumulation can occur in the absence of Canx (**Figure 12B**). MEFs lacking *Canx* or *Crt* (*Calreticulin*) expression had an impaired PC1 delivery to lysosomes. Similarly, MEFs lacking ERp57, a protein disulfide isomerase that cooperates with CANX and CRT to ensure a proper folding of proteins [70], also showed a defective PC1 delivery to lysosomes (**Figure 12D**). The binding of CANX and CRT to target substrates occurs through the recognition of monoglucosylated oligosaccharide residues generated either by ER glucosidases I and II or by UDP-glucose:glycoprotein glucosyltransferase (UGT1) proteins [71, 72].

Pharmacological inhibition of glucosidase activities with Castanospermine (CST) or deletion of Ugt1 in MEFs also inhibited PC1 delivery to lysosomes (**Figure 12D**). These data indicate that all the components of the CANX/CRT cycle are required to operate the PC folding quality control and to select the misfolded PC destined to autophagy.
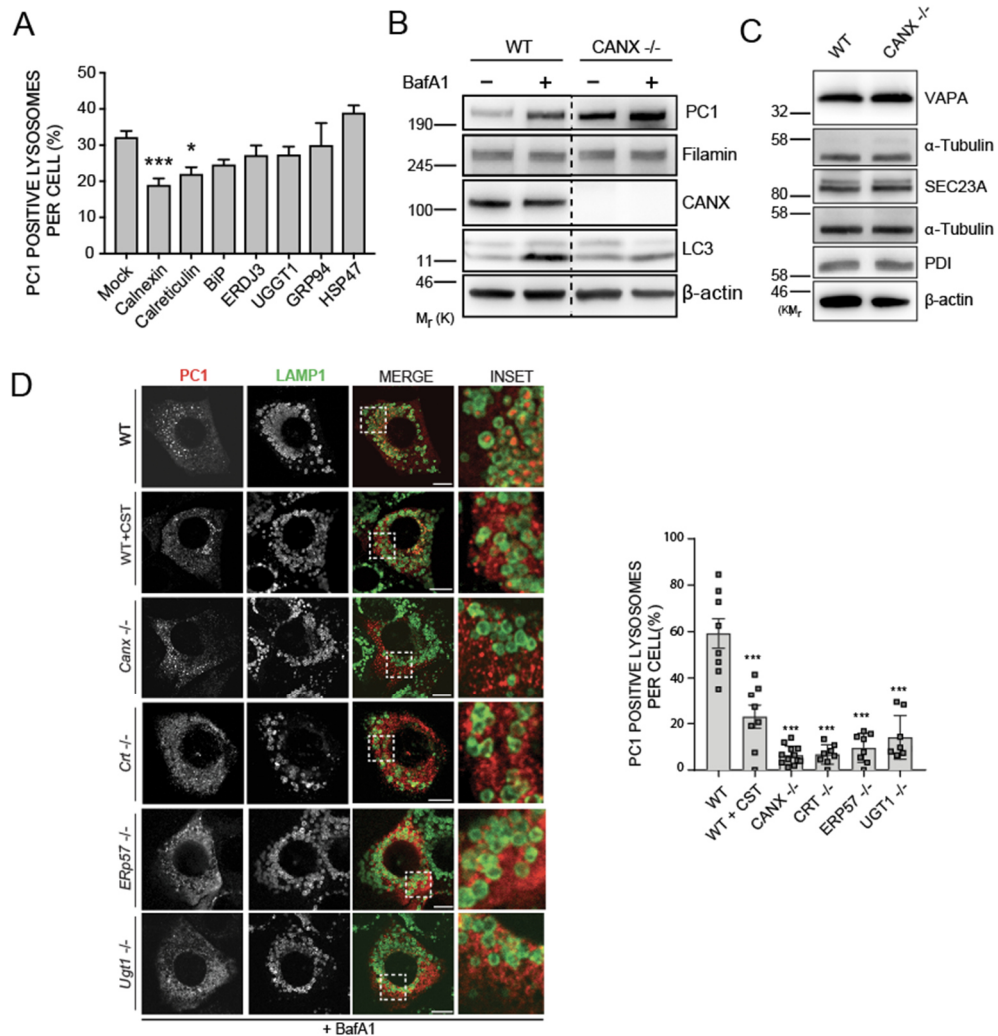
Figure 12. CANX is required for autophagic targeting of ER luminal PC1 and its deficiency fails to increase accumulation of other ER resident proteins.

(**A**) Bar graph shows quantification of lysosomes (LAMP1$^+$) containing PC1 expressed as % of lysosomes (mean +/- SEM) in Saos2 cells mock transfected or transfected with SiRNA against the indicated genes, treated with 100 nM BafA1 for 9h. n=18 cells/treatment; 3 independent experiments. One-way ANOVA (P<0.0001) with Dunnett's multiple comparisons test performed, * P<0.05, *** P=0.0002. (**B**) WT and *Canx*$^{-/-}$ MEFs were left untreated or treated with BafA1 (10 μM) for 6 h, lysed and analysed by western blot with indicated antibodies. Filamin and β-actin were used as loading control. Dashed line indicates

that unnecessary lanes were removed. Western blot is representative of 3 independent experiments. (**C**) WT and KO MEFs for indicated genes were lysed at steady state and analysed by western blotting. Bands were visualised with antibodies against VAPA, SEC23A and PDI. α-tubulin or β-actin were used as controls. Western blots are representative of 3 independent experiments. (**D**) MEF cell lines knock-out or CRIPSR-Cas9 for indicated genes were treated for 12h with 50 nM BafA1 fixed and immunolabeled for PC1 (568, red) and LAMP1 (488, green). CST was added where indicated. Scale bar = 10 μm. Inset panels show magnification of the boxed area. Bar graph shows quantification of LAMP1 vesicles positive for PC1, expressed as % of total lysosomes (mean +/- SEM), n=8, 8, 12, 8, 8, 8 cells respectively; 3 independent experiments. One-way ANOVA with Dunnett's multiple comparisons test performed and P value adjusted for multiple comparisons. *** P<0.0001.

Procollagens are the main substrates that accumulate in Fam134b$^{-/-}$ and Canx$^{-/-}$ cells

Quantitative proteome analysis was performed using Mass Spectrometry (MS) label-free protein quantification approach in *Canx$^{-/-}$* and *Fam134b$^{-/-}$* MEFs versus wild-type MEFs. *Canx$^{-/-}$* and *Fam134b$^{-/-}$* samples were prepared and run in parallel to minimize the variability due to the MS calibration and sample preparation. We identified 95 upregulated and 142 downregulated proteins in *Fam134b$^{-/-}$* MEFs. Specifically, both Col1a1 and Col1a2 peptide chains were among the most significantly increased (–Log Student's T-test p value: 8.55 and 8.2, respectively for Col1a1 and Col1a2) (**Figure 13A**). Gene ontology analysis confirmed the accumulation of collagens in MEFs lacking FAM134B (**Figure 13C**). In *Canx$^{-/-}$* cells, we identified 384 upregulated and 278 downregulated proteins. Col1a1 and Col1a2 peptides were identified as significantly increased also in *Canx$^{-/-}$* MEFs (–Log Student's T-test p value: 3.06 and 2.37, respectively for Col1a1 and Col1a2) (**Figure 13B**). Interestingly, only 17 identified peptides were commonly upregulated in both *Fam134b$^{-/-}$* and *Canx$^{-/-}$* MEFs. Among these, collagens (Col1a1, Col1a2, Col6a1, Col6a2, Col5a1) and collagen interacting proteins (Procollagen C-endopeptidase enhancer 1,

SPARC/Osteonectin) were the most represented categories (**Figure 13D**). These data show

that FAM134B and CANX are important regulators of PC proteostasis and that they might

cooperate for the selective removal of misfolded procollagens in the ER.
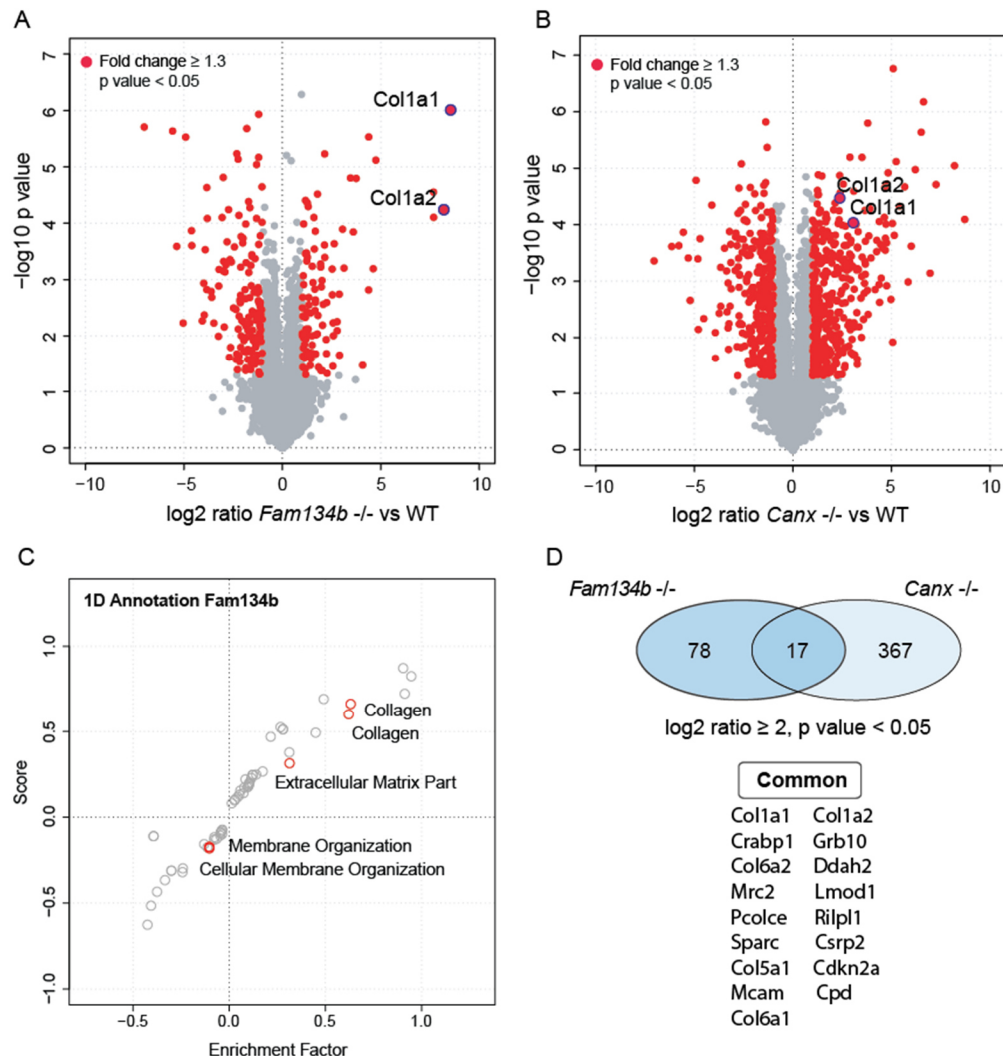
Figure 13. PCs are the main substrates of Fam134b$^{-/-}$ and Canx$^{-/-}$ cells.
(**A, B**) Volcano plot comparing protein fold changes between WT versus *Fam134b$^{-/-}$* (**A**)
and WT versus *Canx$^{-/-}$* MEFs (**B**). Significantly regulated proteins are labelled in red (log$_2$
fold change > 1, –log$_{10}$ p>1.3). Red dots with blue ring indicate collagen 1 peptides. Graphs
represent statistics from three separate experiments for each genotype. (**C**) Scatter plot for
1D annotation enrichment analysis of significantly up-regulated peptides in the *Fam134b$^{-/-}$*
MEFs proteome. (**D**) Venn diagrams represent the number of identified peptides
significantly enriched in *Fam134b$^{-/-}$* (left) and *Canx$^{-/-}$* MEFs (right). List of peptides
upregulated in both *Fam134b$^{-/-}$* and *Canx$^{-/-}$* MEFs.

33

A CANX-FAM134B ER-phagy complex acts as PC autophagy receptor

Mass spectrometry analysis identified CANX as a putative FAM134B interactor [46]. We confirmed this interaction by co-immunoprecipitation experiments. CANX has a N-terminal ER luminal domain, a single transmembrane helix and a short acidic cytoplasmic tail. FAM134B instead is composed of an N-terminal cytosolic domain, a reticulon homology domain (containing alpha helices and a cytosolic loop) and a C-Terminal cytosolic domain (**Figure 14A**). Thus, CANX and FAM134B could potentially interact either in the cytosol or in the ER membrane. We found that the interaction between CANX and FAM134B is lost when co-IP experiments were performed using a mutant version of FAM134B that lacked the intramembrane part of the reticulon homology domain, suggesting that FAM134B interacts with CANX in the ER membrane (**Figure 14B**). Notably, the FAM134Blir mutant still interacts with CANX in co-IP experiments (**Figure 14B-C**).

FAM134B-CANX interaction was not modulated by PCs, since it occurs in HeLa (Kyoto) cells that do not express significant amounts of collagens [73] (**Figure 14D**). Functionally, CANX is not required for FAM134B-mediated ER-phagy, as FAM134B is recruited to LC3-positive vesicles with the same efficiency in both *Canx*$^{-/-}$ and WT MEFs (**Figure 14E-F)**.

We postulated that FAM134B interacts with misfolded PC molecules via CANX. To test this hypothesis, we generated a human osteosarcoma cell line (U2OS) expressing PC2 molecules tagged with HALO at the N-terminus. HA-resin mediated pull down experiments using HA tagged FAM134B or FAM134Blir showed that both HALO-PC2 and CANX interact with FAM134B, irrespective of whether it contained the LIR domain or not (**Figure 14C**). Conversely co-precipitation of LC3II was dependent on a functional LIR motif in FAM134B (**Figure 14C**), consistent with previous results [41]. Castanospermine treatment diminished the level of HALO-PC2 co-precipitated by FAM134B-HA (**Figure 14C**) without perturbing the co-precipitation of CANX and LC3II. Taken together these data suggest a

model by which the interaction of PC with FAM134B is mediated by CANX and that the selective degradation of PC mediated by FAM134B is dependent on PC binding to CANX.
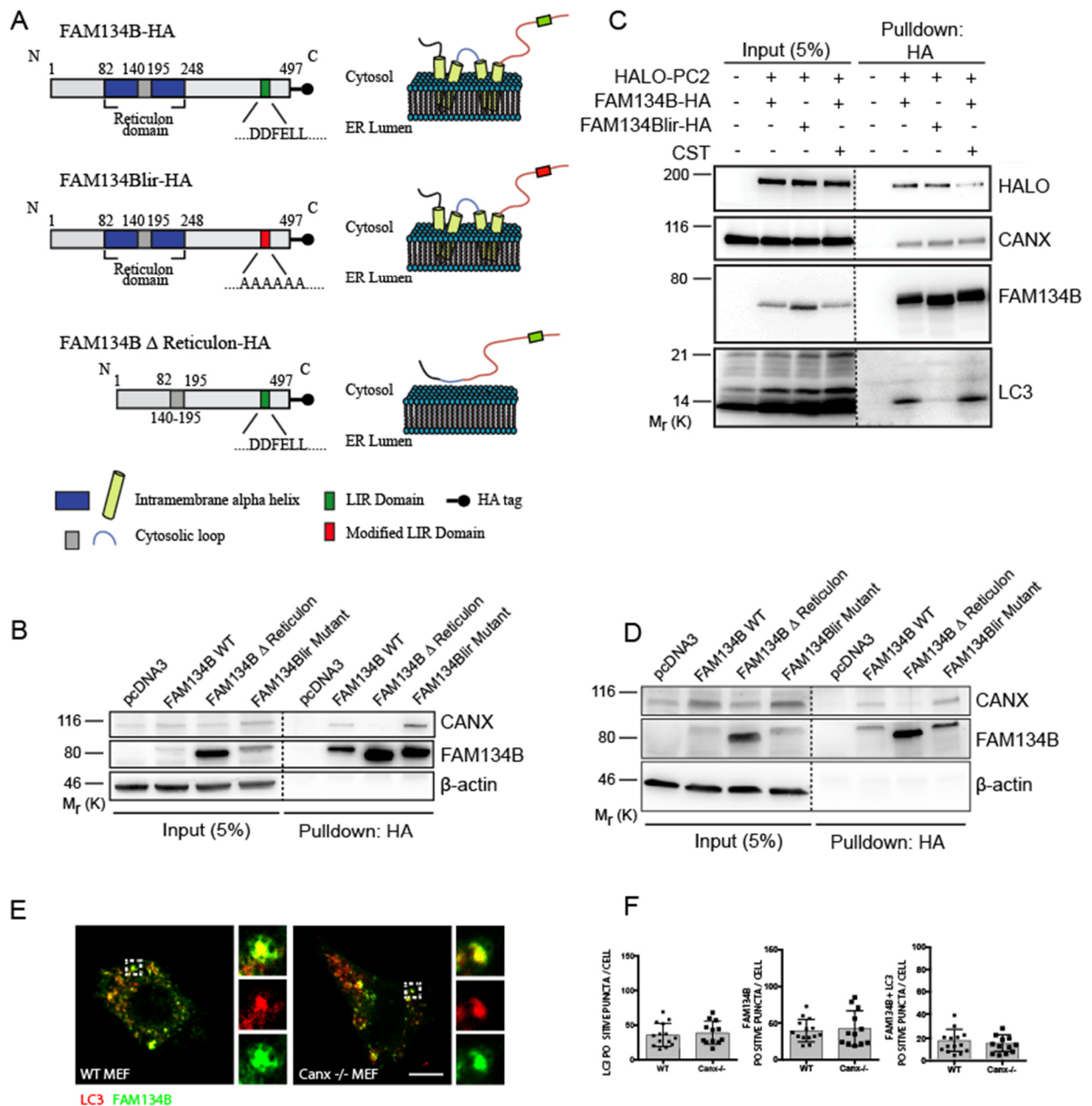
Figure 14. CANX and FAM134B interact and deliver PC1 to autophagosomes. This interaction is not modulated by PC.

(**A**) Schematic representation of FAM134B WT, lir mutant and delta reticulon constructs. (**B, C**) (**B**) U2OS cells were transfected with empty vector control (pcDNA3), FAM134B-HA WT or mutant constructs as indicated. (**C**) U2OS cells transfected with HALO-PC2, and mock transfected or transfected with FAM134B-HA or FAM134Blir-HA constructs, treated with 100 nM BafA1 for 6h and CST where indicated; Complexes were immune-isolated

with HA-magnetic beads, separated by western blot and visualised with antibodies against HALO, CANX, FAM134B, LC3 and β-ACTIN. 5% of the input is shown. Western blots are representative of 3 independent experiments. Dashed line indicates that unnecessary lanes were removed. (**D**) HeLa (Kyoto) cells were transfected with empty vector control, FAM134B-HA WT or mutant constructs as indicated. Complexes were immune-isolated with HA-magnetic beads, separated by western blot and visualised with antibodies against CANX, FAM134B and β-ACTIN. 5% of the input is shown. Western blots are representative of 3 independent experiments. (**E**) Representative immunofluorescence of WT and *Canx*$^{-/-}$ MEFs that were transiently transfected with RFP-LC3 (red) and GFP-FAM134B (green). Scale bar = 10 μm. (**F**) Quantification of AVs positive for RFP-LC3 (red) containing FAM134B (green) expressed as % of total LC3, FAM134B and FAM134B+LC3 per cells (mean +/- SEM). n= 12 cells counted per condition; 3 independent experiments.

Discussion

The FAM134B-CANX complex as a clearing mechanism for PC

In this work we have shown the mechanism by which autophagy selectively recognizes PC molecules destined for degradation in the ER. We have shown that the ER transmembrane chaperone CANX interacts with FAM134B and LC3, forming a novel ER-phagy complex with specific protein targeting capabilities. This complex is responsible for a specific ER-clearance mechanism of PCs, and links a non-native large protein within the ER lumen to the cytosolic autophagy machinery (**Figure 15**).
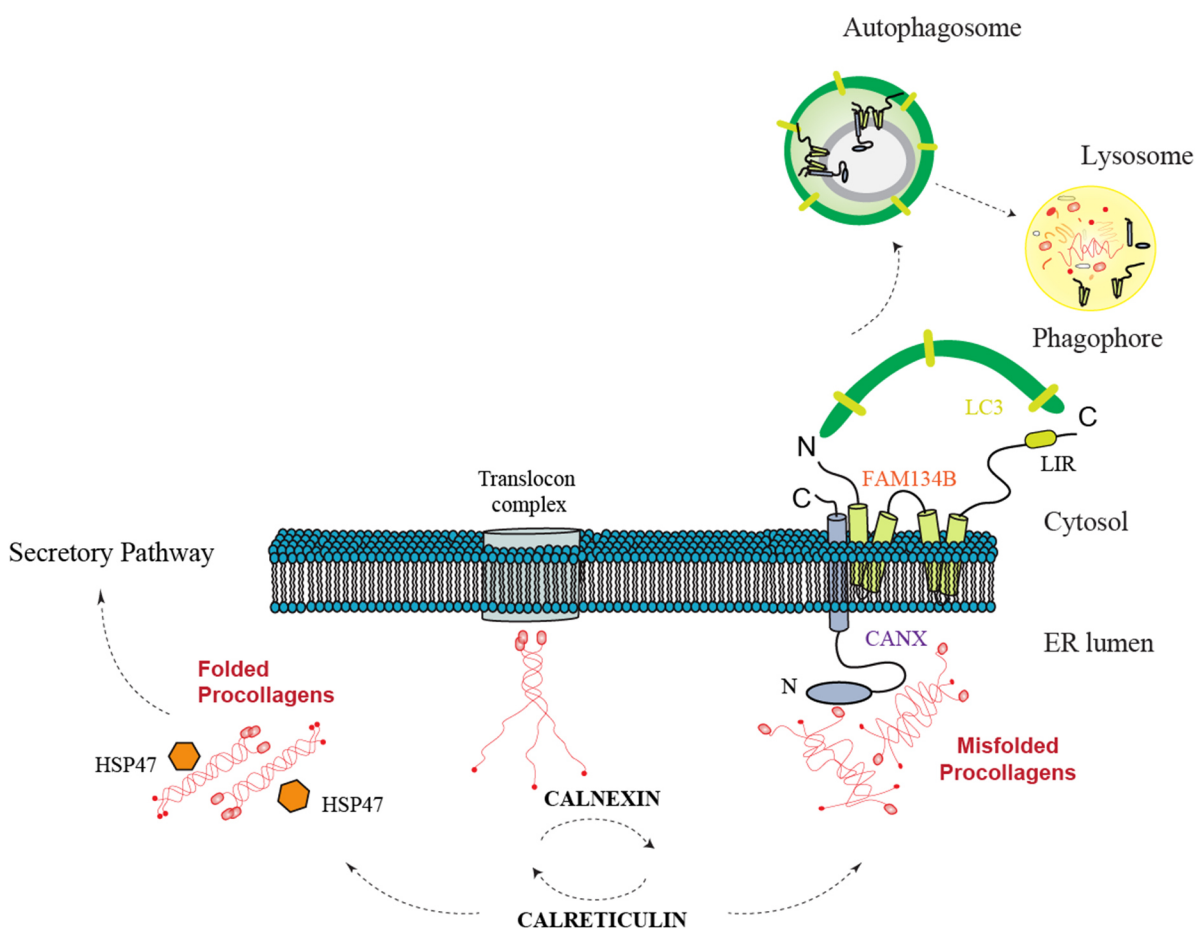
Figure 15. Proposed model of collagen recognition by autophagy.
After synthesis, PC chains are subjected to the quality control operated by the CANX/CRT chaperone system. Properly folded PCs associate with HSP47 and they are then secreted. On the contrary, the misfolded fraction is sequestered by CANX-FAM143B complex and it is delivered to the lysosomes through ER-phagy for degradation.

Firstly, we have found that the all the autophagy machinery is important in PC delivery to the lysosomal system. In fact, we have identified that silencing genes belonging to functionally different complexes involved in autophagosome biogenesis inhibited lysosomal delivery of PCs. Secondly, we have identified the importance of the ER-phagy receptor FAM134B in mediating PC delivery to the lysosomes. FAM134B was recently identified as a receptor that mediates turnover of ER portions via autophagy [41]. These data suggest that FAM134B-dependent ER-phagy also functions as an ER quality control pathway for PCs. In fact, quantitative proteomic analysis in $Fam134b^{-/-}$ MEFs suggests that PCs are the main clients of FAM134B-mediated ER-phagy. Lastly, we have shown that the ER chaperone CANX represents an important player in PC disposal via ER-phagy. CANX is a molecular chaperone that assists the folding of monoglucosylated glycoprotein in the ER. CANX forms transient complexes with unfolded ER proteins until they either become folded or are degraded [74]. Our data demonstrated that the genetic or pharmacological inhibition of ER enzymes that mediate the binding of substrates to CANX impaired the PC delivery to the lysosomes. This suggests that the N-glycans-mediated recognition of PC by CANX (and CRT) is a prerequisite for PC targeting to autophagosomes. Consistently co-immunoprecipitation experiments demonstrate that PC2 binding to FAM134B complex depends on CANX substrate affinity, since it can be reduced by CST treatment. Finally, we have also provided biochemical evidence indicating that FAM134B interacts with CANX via the transmembrane reticulon homology domain. The reticulon homology domain generates membrane curvature and remodelling by increasing the area of the cytoplasmic leaflet [75]. The observation that CANX-FAM134B binding is rather stable and not modulated by PCs suggests that the binding of PC to CANX might induce a conformational change of the FAM134B reticulon homology domain that increases ER membrane curvature, favouring vesicle formation. Indeed, CLEM analysis confirmed the presence of both PC molecules and CANX within a small vesicle contained within a large autophagosome,

supporting the model by which portions of the ER containing both CANX and PC are sequestered into autophagosomes. These data overall show the importance of FAM134B-mediated ER-phagy in maintaining cellular proteostasis and degradation for procollagen molecules.

The FAM134B-CANX complex as a clearing mechanism for additional proteins

FAM134B has recently emerged also in the lysosomal degradation of a mutant form of alpha1-antitrypsin Z (ATZ), together in complex with CANX [34]. The pathway identified for the proteasome-resistant ATZ was named ER-to-lysosome associated degradation (ERLAD). In ERLAD, the protein aggregates of ATZ are first segregated in ER subdomains, then enclosed in transport vesicles that eventually fuse with lysosomes for degradation (**Figure 16**). It shows substantial differences compared to the quality control autophagy of endogenous PC. Firstly, the delivery of PC molecules to lysosomes fully relies on autophagosome formation and on components of the autophagosome biogenesis machinery. Conversely, many of them (e.g. ULK1/2, ATG9 and ATG13) are dispensable for ERLAD, suggesting that the CANX-FAM134B complex can mediate ER cargo clearance though different vesicular pathways. Secondly, both in quality control autophagy of PC and ERLAD, the ER chaperone CANX delivers the misfolded cargo in ER subdomains to be cleared from cells on stable interactions with FAM134B. However, other components of the CANX chaperone system (i.e., CRT, UGT1 and ERp57) cycle are required in quality control autophagy of PC, but are dispensable for ERLAD. These results highlight the complexity of quality control pathways operating in mammalian cells to surveil the ER lumen and prevent accumulation of misfolded proteins in the ER. All in all, FAM134B has emerged to have a crucial role in controlling cellular proteostasis operating in different ER quality control pathways and involving many ER clients, including PC and ATZ.
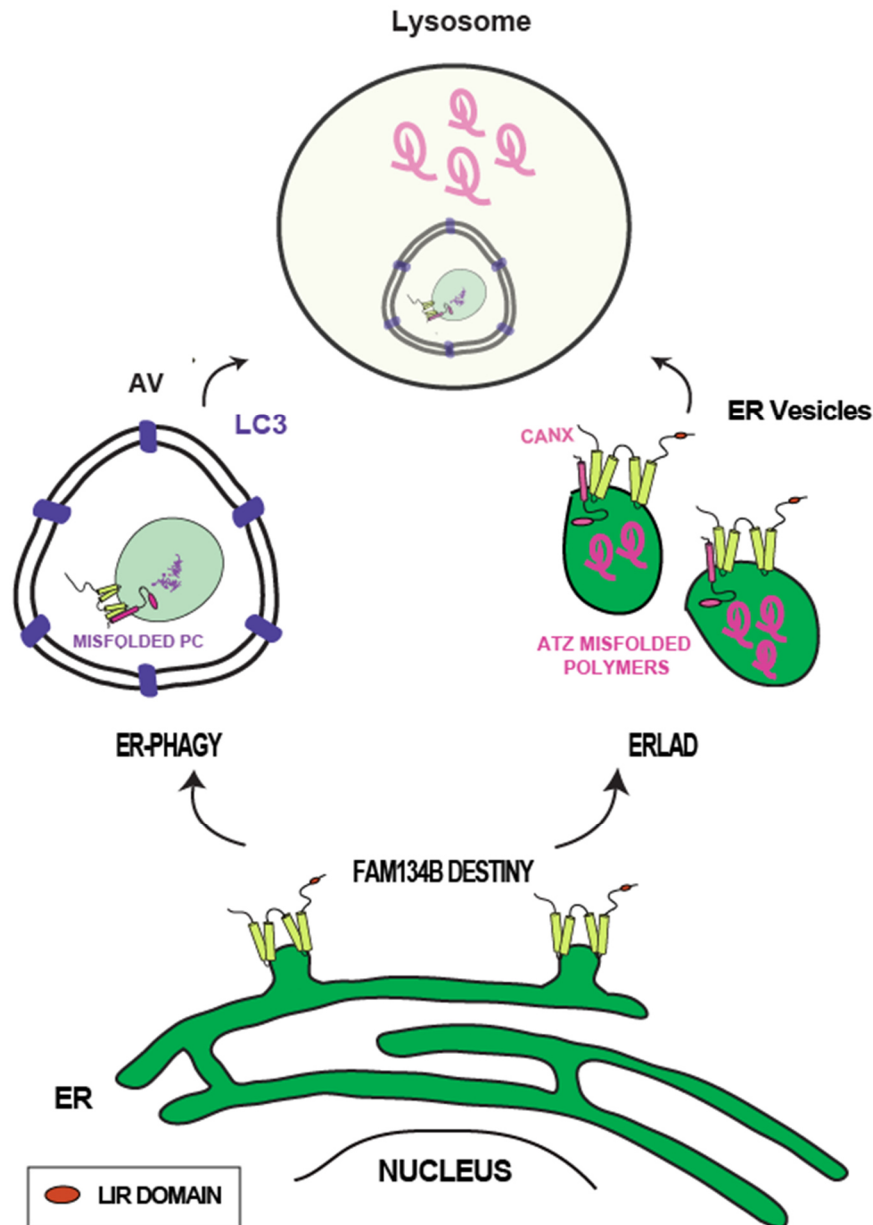
Figure 16. The possible routes of FAM134B-mediated vesicular transport for cargo degradation.

The ER-resident receptor FAM134B transits from the ER via different routes: via ER-phagy (for the selective degradation of procollagen) and via ER-to-lysosome associated degradation (ERLAD, for the selective degradation of alpha1-antitrypsin Z). In ER-phagy, the PC delivery to the lysosomes requires autophagosomes, LC3 positive (in blue). In ERLAD, the protein aggregates of ATZ are first segregated in ER subdomains, then enclosed in ER single-membrane transport vesicles that eventually fuse with lysosomal degradative organelle, not requiring autophagosome formation. Abbreviations: ER, endoplasmic reticulum; PC, procollagen; AV, autophagic vesicle; CANX, Calnexin; ATZ, alpha1-antitrypsin Z; LIR domain, LC3 interacting region.

Alternative pathways of degradation for PC molecules

Procollagen molecules are degraded via at least three different collagen quality control pathways that operate during the different steps of procollagen production in the ER (**Figure 17**). The first mechanism of PC degradation to be described is operated by ERAD, for single procollagen chains that are not yet trimerized [21]. The second, herein described operated by ER-phagy, during trimerization and mediated by the Calnexin and related chaperones. However, a third pathway is emerged for PC degradation, operated by microautophagy at level of ER-exits sites prior secretion [33]. PCs destined to secretion leave the ER through sub-regions called ER exit sites (ERESs) via coat protein complex II (COPII)-coated vesicles [59, 76]. The ERESs represent very specialized ER zones for the transport of cargo proteins from the ER to the Golgi apparatus and are highly regulated [76]. Misfolded procollagens have been shown to accumulate at the ER exit sites, that are then engulfed by lysosomes through a microautophagy-like mechanisms, not involving conventional, double-membrane autophagosomes [33]. Of note, this described process for PC degradation may ensue at an earlier stage of PC trafficking, occurring at the ERESs, so that overall only properly folded PCs enter the secretory pathway.
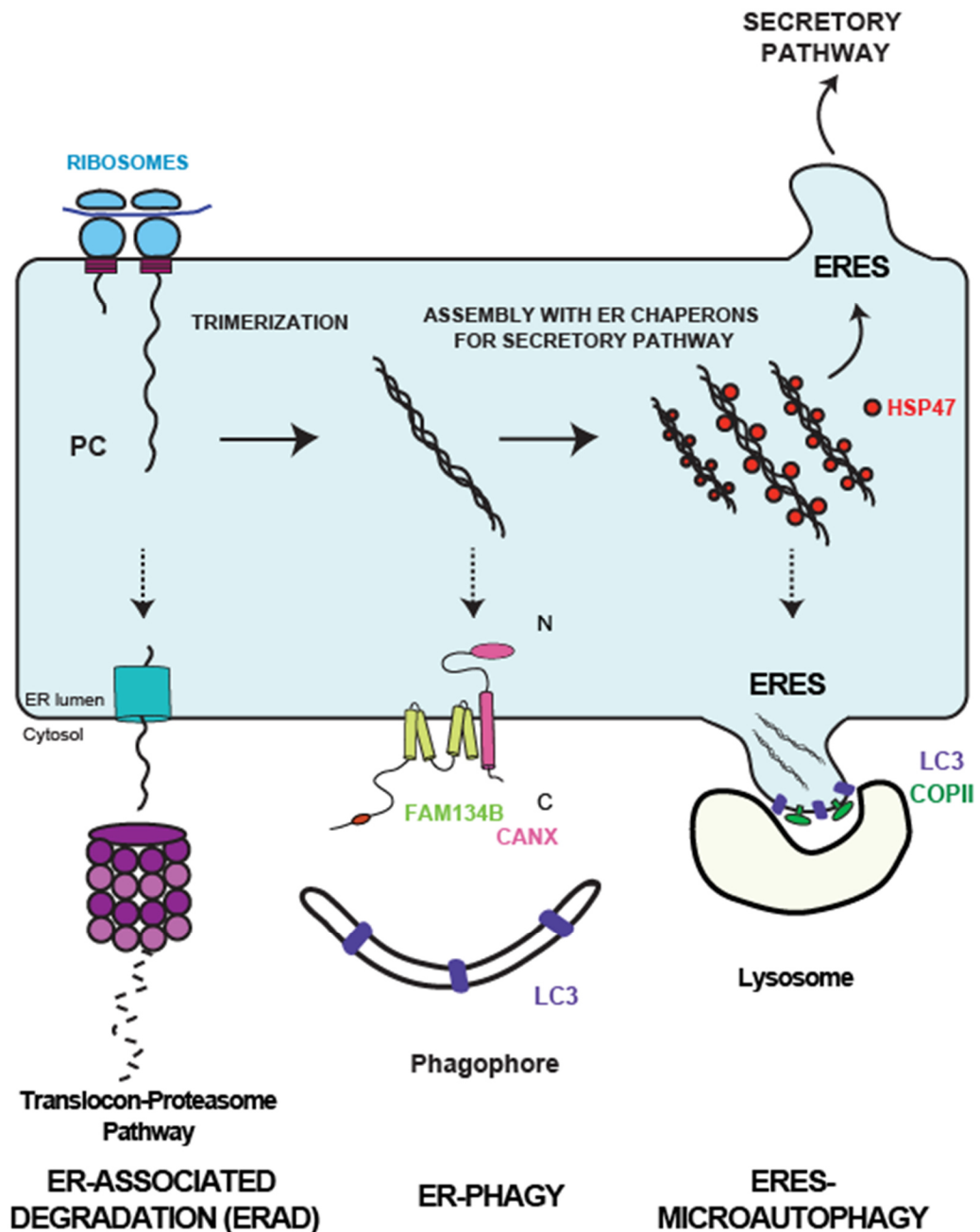
Figure 17. PC quality control pathways at the ER.

Distinct PC quality control exists operating during the different steps of PC production in the ER: **ER-associated degradation**, for degradation of single procollagen chains. **ER-phagy**, during trimerization and mediated by the FAM134B-Calnexin complex. **Microautophagy** at level of ER-exit sites prior secretion. Continuous lines represent folded PC molecules at the ER during different steps, from biosynthesis to secretion. Dashed lines represent misfolded collagen delivered to degradative pathways. Abbreviations: PC, procollagen; N, N-terminal domain; C, C-terminal domain; ERES, ER-exit sites; CANX, Calnexin; Lys, lysosome; AV, autophagic vesicle; COPII, COPII vesicles.

Concluding Remarks

The FAM134B-mediated ER-phagy plays different cellular functions, from maintaining ER homeostasis and size to the selective removal of specific cargoes from the ER. The impairment of ER-phagy leads to a lack of ER homeostasis and protein accumulation, representing a primary pathogenic cause for a number of human diseases. Therefore, the identification of the underlying mechanisms related to the ER-phagy is fundamental to develop potential therapeutic targets to tackle potentially this pathway in human disorders, such as conformational diseases.

Materials and Methods

Cell culture, transfections, siRNA and plasmids

Cell culture: Mouse Embryonic Fibroblasts (MEFs) and Swarm Rat Chondrosarcoma (RCS) cell lines were cultured in DMEM with 10% FBS and 1% penicillin/streptomycin at 37°C in 5% CO2. Human bone Osteosarcoma (Saos2 and U2OS) cells were purchased from ATCC and cultured in McCoys medium with 15% (Saos2) or 10% (U2OS) FBS and 1% penicillin/streptomycin at 37°C in 5% CO2. For collagen experiments, medium was supplemented with 50 μg/ml ascorbic acid. Wild-type, $Atg7^{-/-}$, MEFs were gifts from M. Komatsu and N. Mizushima. $Atg16^{-/-}$ MEFs were from T. Saitoh. $Fip200^{-/-}$ MEFs were from J.-L. Guan. The generation of the Sec62 CRISPR-Cas9 knockout MEF cell line was previously described [45]. $Canx^{-/-}$ MEF cell lines were previously described [77]. $Fam134b$ CRISPR-Cas9 MEF cell line was generated in [34]. Fam134b$^{-/-}$ MEF cell line was generated in [41]. $Crt^{-/-}$, $Erp57^{-/-}$ and $Ugt1^{-/-}$ were previously described [78-80].

Saos2 IDUA CRISPR-Cas9 cell line: for construction of the guideRNA-Cas9 plasmid, pSpCas9(BB)-2A-Puro plasmid (PX459) (Plasmid #62988) was obtained from Addgene. To clone the guide sequence into the sgRNA scaffold, two annealed oligonucleotides (5'-CACCGCAGCTCAACCTCGCCTATG-3', 5'- AAACCATAGGCGAGGTTGAGCTGC-3') were inserted into the pSpCas9(BB)-2A-Puro plasmid using BbsI restriction site. Saos2 cells were transfected with the plasmid using Lipofectamine LTX and Plus Reagent (Invitrogen, Thermo Fisher Scientific) following a reverse transfection protocol. Two days after transfection, the medium was supplemented with 1 μg/ml puromycin. Puromycin-resistant clones were isolated and gene KO was verified by sequencing. CRISPR *IDUA* and WT Saos2 cells were kept in medium containing 1 mg/ml dermatan sulphate (Sigma-Aldrich) for 48 hours before any experiment was performed.

Transfection: Cells were reverse transfected using Lipofectamine LTX and PLUS reagent (Invitrogen) according to manufacturer's instructions. For siRNA experiments, siGENOME

SMARTpool siRNAs (Dharmacon Thermo Scientific) were transfected to a final concentration of 100 nM and cells harvested 72h after transfection.

Plasmids: GFP–LC3 was from Dr. Yoshimori. GFP-DFCP1 was from Dr. Tooze. FAM134Blir-HA and FAM134BΔReticulon-HA expression plasmids were from Prof. Ivan Dikic. HALO-PC2 plasmid was generated as follows: pLT007, a vector for CMV promoter-driven expression of N-terminally Halo-tagged Col2a1 was created by replacing the mCherry tag with the Halo tag in the mCHERRY-C2-COL2A1 plasmid [81]. Standard techniques were used for construction, transformation and purification of plasmids. FAM134B-GFP was previously described [41]. Site directed mutagenesis plasmids: R789C and G1152D mutations were created using the Agilent Quikchange XL Site-Directed mutagenesis kit using the mCherry-PC2 backbone.

Primer sequences were designed with PrimerX online software and were as follows: R789C forward: 5' CGGTCTGCCTGGGCAATGTGGTGAGAGAGGATTC 3' and reverse: 5' GAATCCTCTCT CACCACATTGCCCAGGCAGACCG 3'; G1152D forward: 5'GGTCCTTCTGGAGACCAAGATGCTTCTGGTCCTGCTGG 3' and reverse: 5' CCAGCAGGACCAGAAGCATCTTGG TCTCCAGAAGGACC 3'.

Immunofluorescence

Cells were seeded on coverslips at least 24h before treatment and fixed for 10 min in 4% PFA, or for the detection of endogenous LC3, fixed for 10 min in ice-cold methanol. Cells were blocked and permeabilized for 30 min in blocking buffer (0.05% (w/v) saponin, 0.5% (w/v) BSA, 50 mM NH_4Cl and 0.02% NaN_3 in PBS, pH 7.2-7.4). For LAMP1 immunolabeling, 15mM glycine was added to blocking buffer. Cells were incubated for 1h with the following primary antibodies: COLLAGEN I (SP1.D8, Hybridoma Bank), COLLAGEN II (II-II6B3; Hybridoma Bank), LAMP1 (Abcam, ab24170) or LAMP1 (Hybridoma Bank, 1D4B), CANX (Enzo Life Sciences ADI-SPA-860-D), LC3 (NB100-

2220; Novus Biologicals), HSP47 (Abcam, ab77609); HA (Sigma, H6908), washed 3 times in PBS; incubated for 45 min with secondary antibody (Alexa Fluor–labelled goat anti-rat A11077, goat anti-guinea pig A11073, goat anti-rabbit A11011/A11008, and goat anti-mouse A11001, A11004; Life Technologies, Thermo Fisher Scientific); washed 3 times in PBS; incubated for 20 minutes with 1 µg/ml Hoechst 33342, and finally mounted in Mowiol (Sigma-Aldrich) or Vectashield (Vector Laboratories) supplemented with 40,6-diamidino-2-phenylindole (DAPI) .

Medaka stocks

Samples of the Cab strain of wild-type medaka fish were kept and staged as described previously [82, 83]. All studies on fish were conducted in strict accordance with the institutional guidelines for animal research and approved by the Italian Ministry of Health; Department of Public Health, Animal Health, Nutrition and Food Safety in accordance to the law on animal experimentation (article 7; D.L. 116/92). Furthermore, all animal treatments were reviewed and approved in advance by the Ethics Committee at the TIGEM Institute [Pozzuoli (NA), Italy].

Immunofluorescence analysis in Medaka fish embryos

The animals were subjected to anaesthesia before fixation at stage 40 by two hours of incubation in Methanol 100% at room temperature (RT). Samples were rinse three times with PTw 1X (1xPBS, 0.1% Tween, pH 7.3) and then incubated overnight in 15% sucrose/PTW1X at 4°C, and then again incubated overnight in 30% sucrose/PTW1X at 4°C. Cryosections of the larvae were processed for immunostaining. Specifically, cryosections were rehydrated in PBS1X for 30 minutes, washed in PBS-0.1% Triton X-100 and treated with antigen retrieval solution [proteinase K 20mg/ml (Sigma Aldrich, Germany) dissolved in 10 mM TRIS pH 8.0, 1mM EDTA (TE)] for 15 minutes at 37°C. Cryosections were then

permeabilized with 0.5% Triton X-100 in PBS1X for 20 minutes at RT, rinsed in PBS 0.1% Triton X-100 and moved to blocking solution [2% BSA, 2% serum, 2% DMSO in PBS-0.1% Triton X-100] for 30 minutes at RT. Cryosections were incubated with rabbit anti-Collagen Type I (1:400) and mouse anti-LC3B (Nanotools, 1:100) antibodies over night at 4°C. Cryosections were washed with PBS-0.1% Triton X-100 and incubated with secondary antibodies, Alexa-594 anti-rabbit IgG (1:500), Alexa-488 anti-mouse IgG (1:500) (Thermo Fisher) for one hour at RT. Nuclei were stained with DAPI (1:500).

Chemicals and cell treatments

L-Ascorbic acid (Sigma-Aldrich) was made fresh and used at a final concentration of 50 µg/ml from the beginning of each experimental procedure. Bafilomycin A1 (BafA1) (Sigma-Aldrich) was used at a final concentration of 100 nM, and compared to DMSO (Sigma-Aldrich) as vehicle for 6h (RCS) or 9h (Saos2/U2OS). MEFs were treated with 50nM Bafilomycin for 12h or 100nM for 6h. For Bafilomycin washout experiments, BafA1 was added 100nM for 4 h, followed by 4 h washout adding medium without BafA1. Castanospermine (CST) (Sigma-Aldrich) was used at a final concentration of 1 mM. CST was added 2h before BafA1 and ascorbic acid treatment. Tat-BECLIN1 (D17, Millipore) was used at 5µM in acidified media for 4 h, then replaced with fresh media for 2 h before harvesting the cells. SAR405 (Selleckchem) was used at a concentration of 10 µM for 2 hours preceding and throughout BafA1 treatment. HALO-tag, far red (ex. 650 nm, em. 668 nm) SiR HaloTag ligand (Promega), available through custom order, incubated in media at 2 mM for 3 h. 0.5 µM TMR (Promega) was added to the media 2h pre-fixation for lysosome visualisation, or for pulse chase, 20 min at 1 µM, followed by p5030 (Promega). Rutin (Acros Organics) was used at 10 µg/mL for the duration of live cell imaging.

Confocal Microscopy

Scanning laser confocal experiments were acquired using a Zeiss LSM 800 confocal microscope equipped with a 63 × 1.4 numerical aperture oil objective. Airyscan microscopy was performed using a Zeiss LSM 880 confocal microscope, equipped with Plan-Apochromat 63x/1.4 numerical aperture oil objective and pixel size of 8.7nm. Images were subjected to post-acquisition airyscan processing. Image acquisition and processing was performed with Zen Blue software and colocalization analysis and image presentation was performed using ImageJ FIJI software.

Live Cell Imaging

U2OS cells were transiently transfected with mCherry-PC2 and RDEL-HALO plus GFP-LC3. Cells were incubated on a Tokai Hit stage top incubator heated stage in 5% CO_2 at 40 °C in the presence of far red HALO ligand for 3 h. Immediately prior to imaging, medium was supplemented with ascorbic acid and rutin (routinely used to decrease photobleaching). Imaging was initiated at temperature switch to 32 °C. Frames were acquired at 1 s intervals. Imaging was performed on a Nikon Inverted Spinning Disk confocal with sCMOS Prime95B camera (Photometrics) with pixel size of 11 μm, using a 100x CFI Plan Apo oil objective with 1.4 NA. Image acquisition was performed with Metamorph 7.7.6 software (Molecular Devices, France) and processing in ImageJ FIJI software.

Correlative light-electron microscopy (CLEM) and Tomography

Saos2 cells were grown on gridded MatTek glass bottomed dishes (MatTek Corporation) transfected with GFP-LC3 and fixed with 0.05% glutaraldehyde in 4% paraformaldehyde (PFA) and 0.1M Hepes buffer for 10 min, washed once in 4% PFA, then incubated in fresh 4% paraformaldehyde in 0.1M Hepes buffer for 30 min. Subsequently, cells were incubated for 30 min in blocking buffer and immunolabeled for collagen I (SP1.D8) and CANX (ADI-

SPA-860-D Enzo Life Sciences), visualized with Alexa-Fluor546 fluoro-nanogold Fab'
conjugate (Nanoprobes) and Alexa-Fluor647 Rabbit Ab respectively. Nanogold was
enlarged using gold enhancement kit (Nanoprobes) according to manufacturer's instructions.
Samples were then postfixed with 1.5% potassium ferricyanide, 1% OsO_4 in 0.1 M
cacodylate buffer for 1 hour on ice and enbloc stained overnight with 1% uranyl acetate.
Samples were dehydrated in ethanol, and embedded in Epoxy resin (SIGMA). After baking
for 48h at 60°C, the resin was released from the glass coverslip by temperature shock in
liquid nitrogen. Serial sections (70–90 nm) were collected on carbon-coated formvar slot
grids and imaged with a Zeiss LEO 512 electron microscope. Images were acquired with a
2k×2k bottom-mounted slow-scan Proscan camera controlled by EsivisionPro 3.2 software.
For electron tomography tilted series were acquired with a 200kV Tecnai G2 20 electron
microscope (FEI, Eindhoven) at a magnification of 11.5k, resulting in pixel size of 1.95nm.
Single, tilted image series (±60° according to a Saxton scheme with the initial tilt step of 2°)
were acquired using Xplorer3D (FEI) with an Eagle 2,048×2,048 CCD camera (FEI). Tilted
series alignment and tomographic reconstructions were done with the IMOD software
package. Image segmentation was done by MIB software (BW thresholding) and visualized
using IMOD.

Transmission Electron Microscopy

Cells were fixed in 1% glutaraldehyde in 0.2 M HEPES buffer and then post-fixed in uranyl
acetate and in OsO_4. After dehydration through a graded series of ethanol, samples were
cleared in propylene oxide, embedded in Epoxy resin (Epon 812) and polymerized at 60°C
for 72h. From each sample, thin sections were cut with a Leica EM UC6 ultramicrotome and
images were acquired using a FEI Tecnai −12 (FEI) electron microscope equipped with
Veletta CCD camera for digital image acquisition.

Immunoprecipitation experiments

HA-tag precipitation: U2OS cells were transiently transfected with plasmids encoding HALO-PC2 and FAM134B-HA. On the day of experiment, plates were treated with 1mM CST where indicated for 2h, then all plates treated with 100nM BafA1 and 50 µg/ml ascorbic acid for 4h. Cells were detached with Tripsin-EDTA and centrifuged. The cell pellets were washed three times with ice-cold PBS, then resuspended in 1mL MCLB lysis buffer (1% NP-40, 150mM NaCl, 50mM Tris HCl pH8). The cell suspension was lysed by passing it through a 24G needle for 10-15 times. The lysates were incubated on ice for 20 minutes with gentle swirling and centrifuged at 14000rpm to pellet nuclei and cell debris. The supernatants were collected and subjected to protein quantification using BCA protein assay kit (Pierce Chemical). 1mg of each lysate was then precipitated using Pierce anti-HA magnetic beads (Thermo Fisher Scientific) and rotated at 4°C overnight. The precipitated proteins were washed three times with MCLB lysis buffer (1% NP-40, 150mM NaCl, 50mM Tris HCl pH8) and two times with the same lysis buffer, detergent free. The protein complexes were resuspended in 1v/v 2X Laemli Sample buffer and analysed by SDS-PAGE in a 7-14% gradient gel.

HeLa (Kyoto) cells and U2OS cells were transiently transfected with empty vector control, FAM134B-HA WT or mutant constructs. On the day of the experiment cells were detached with Tripsin-EDTA and centrifuged. Immunoprecipitation experiments were performed in the same conditions and analysed by SDS-PAGE in a 4–15% Mini-PROTEAN® TGX™ Precast Protein gel.

Western blot analysis

Cells were washed twice with PBS and then scraped in RIPA lysis buffer (20 mM Tris [pH 8.0], 150 mM NaCl, 0.1% SDS, 1% NP-40, 0.5% sodium deoxycholate) in the presence of PhosSTOP and EDTA-free protease inhibitor tablets (Roche). Cell lysates were incubated

on ice for 30 minutes, then the soluble fraction was isolated by centrifugation at 16,000 g for 20 minutes at 4°C. The total protein concentration in cellular extracts was measured by BCA protein assay kit (Pierce Chemical). Protein extracts, separated by SDS-PAGE and transferred onto membranes, were probed with antibodies against COLLAGEN I (Abcam, ab138492 for human cells; Abcam, ab21286 for mouse cells), LAMP1 (Abcam, ab24170), LC3B (NB100-2220; Novus Biologicals), CANX (Enzo Life Sciences ADI-SPA-860-D), HALO (Promega G928A) FAM134B (Sigma, HPA012077), SQSTM1/p62 (Abnova, H00008878-M01), SEC23A (PAI-069A; Thermo Fisher Scientific), VAP-A (15275-1-AP, Proteintech), PDI (Enzo Life Sciences ADI-SPA-891-F), FILAMIN (Abcam, ab76289), TUBULIN (T5168, Sigma-Aldrich) and β-ACTIN (Novus Biologicals NB600-501), probed with horseradish peroxidase (HRP)-conjugated goat anti-mouse or anti-rabbit IgG antibody (1:2,000, Vector Laboratories) (8125, 8114; Cell Signaling Technology) and visualized with the Super Signal West Dura substrate (Thermo Fisher Scientific), according to the manufacturer's protocol.

Mass spectrometry

Wild-type, *Fam134b* and *Canx* knockout MEFs were grown in DMEM media supplemented with 10% FBS. Cells were lysate in SDS-lysis buffer (4% SDS in 0.1M Tris/HCl pH 7.6). Protein concentration was measured using BCA Kit (Pearce) and 50μg of cells lysate was precipitated with ice-cold acetone and re-suspended in 30μl of GnHCl buffer (6M guanidine hydrochloride, 50mM Tris pH 8.5, 5mM TCEP, 20mM chloro-iodoacetamide). For label-free quantification-based proteome analysis of whole cell lysates, proteins were in-solution digested with the endopeptidase sequencing-grade Lys-C (1:100 ratio) for 3h at 37°C and subsequently with Trypsin (1:100 ratio) overnight 37°C. Digestion was blocked with TFA 1% final concentration. Collected peptide mixtures were concentrated and desalted using the Stop and Go Extraction (STAGE) technique [84].

Instruments for LC-MS/MS analysis consisted of a NanoLC 1200 coupled via a nano-electrospray ionization source to the quadrupole-based Q Exactive HF benchtop mass spectrometer (Thermo Scientific). Peptide separation was carried out according to their hydrophobicity on an in-house packed 20cm column with 1.9mm C18 beads (Dr Maisch GmbH) using a binary buffer system consisting of solution A: 0.1% formic acid (0.5% formic acid) and B: 80% acetonitrile, 0.1% formic acid (80% acetonitrile, 0.5% formic acid). 2 hr gradients were used for each sample. Linear gradients from 5–38% B were applied with a following increase to 95% B at 400nl/min and a re-equilibration to 5% B. Q Exactive HF settings: MS spectra were acquired using 3E6 as an AGC target, a maximal injection time of 20ms and a 60,000 resolution at 200m/z. The mass spectrometer operated in a data dependent mode with subsequent acquisition of higher-energy collisional dissociation (HCD) fragmentation MS/MS spectra of the 15 most intense peaks. Resolution for MS/MS spectra was set to 30,000 at 200m/z, AGC target to 1E5, max injection time to 25ms and the isolation window to 1.6 Th.

Statistics

Statistics were performed in Graphpad PRISM software. A two-tailed, paired and unpaired Student's T test were performed when comparing the same cell population with two different treatments or cells with different genotypes, respectively. One-way ANOVA and Dunnett's post-hoc test were performed when comparing more than two groups relative to a single factor (treatment). A P value of 0.05 or less was considered statistically significant.

For mass spectrometry analysis, the raw files were processed using MaxQuant software [85]. Parameters were set to default values. Statistical analysis, T-test and GO annotation enrichment were performed using Perseus software [86]. Data are representative of three independent mass spectrometry analyses for each genotype.

Appendix

Introduction

Although the role of ER-phagy in the regulation of ER size and cellular proteostasis has been well characterized, the upstream signaling pathways regulating ER-phagy in response to cellular needs are still largely unknown.

Of note, chondrocytes reside in an avascular zone with scarcity of nutrients, being the growth plate. During endochondral ossification, these cells are highly secretory synthesizing extracellular matrix components, including collagens and proteoglycans [87]. Therefore, their activity must rely on efficient ER functions. As previously shown, the inhibition of autophagy in chondrocytes was associated to ER dysfunction suggesting that in these cells autophagy is necessary to maintain ER homeostasis, particularly during periods of high demand of protein secretion [61]. Moreover, our group has previously demonstrated that fibroblast growth factor (FGF) signaling is a potent activator of autophagy in chondrocytes [61]. All the above observations have led us to investigate whether FGF triggers a signaling cascade that culminates with the induction of ER-phagy.

Specifically, it has been found that the nutrient responsive transcription factors TFEB and TFE3 - master regulators of lysosomal biogenesis and autophagy [88]- control ER-phagy by inducing the expression of lysosomal genes, involved in lysosomal biogenesis, and the ER-phagy receptor FAM134B. The TFEB/TFE3-FAM134B axis promotes in turn ER-phagy activation upon prolonged starvation. In addition, this pathway has been shown to be activated in chondrocytes by FGF signaling, a critical regulator of chondrocyte differentiation (**Figure 18**).

In this project, I have characterized how the FGF signaling activates the TFEB/TFE3 axis. Specifically, my work has led to identify that the FGF signaling induces a JNK-dependent proteasomal degradation of the insulin receptor substrate 1 (IRS1), which inhibits the insulin-PI3K-PKB/Akt-mTORC1 pathway and promotes TFEB/TFE3 nuclear translocation. In collaboration with the Medaka Facility, I have characterized the effect of FAM134B

knock-down in Medaka embryos. Specifically, the lack of FAM134B impairs cartilage growth and mineralization in medaka fish. The model of the present project is shown in **Figure 18** and the above data are further elucidated in the next sections.
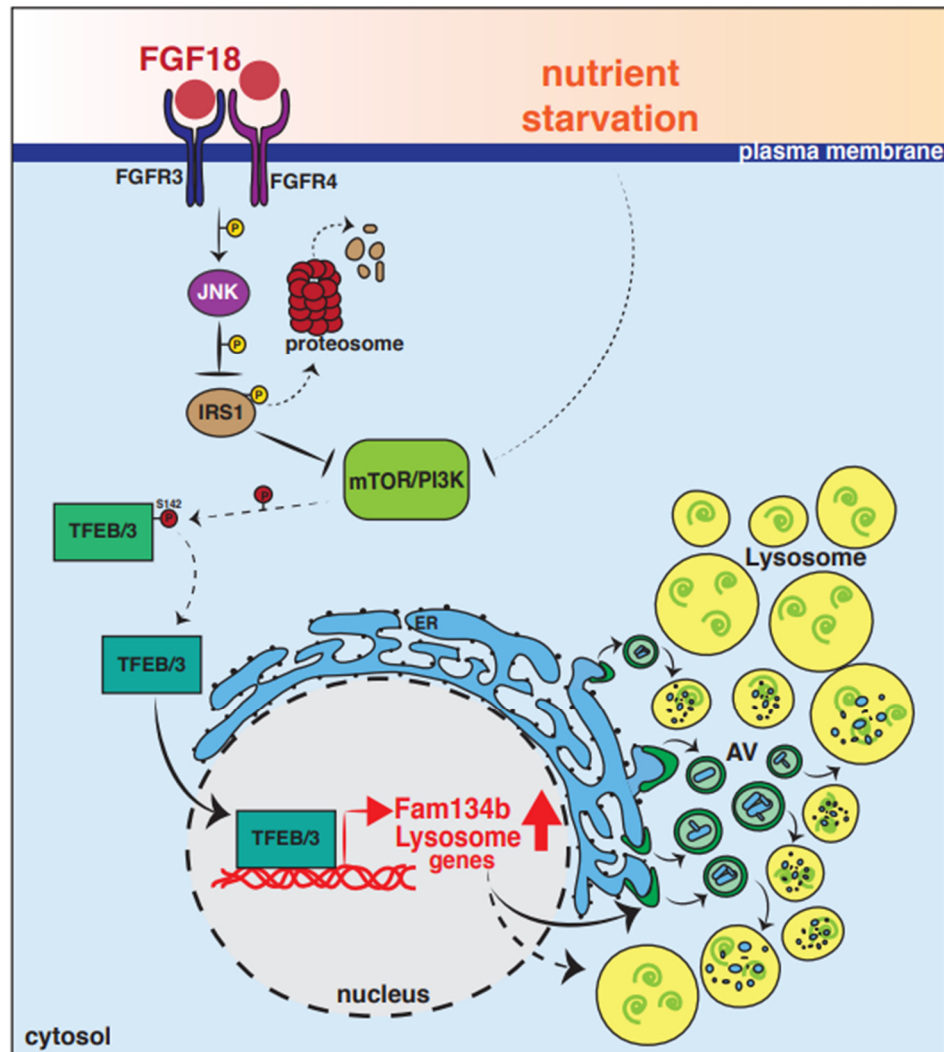
Figure 18. Representative model of induced ER-phagy in chondrocytes.
FGF18, through FGFR3 and FGFR4 receptors, induces JNK-dependent phosphorylation and proteasomal degradation of IRS1 protein, which in turn inhibits the PI3K pathway and promotes TFEB/TFE3 nuclear translocation. In the nucleus, the active transcription factors co-induce the expression of lysosomal, autophagy genes and the ER-phagy receptor Fam134b. Concomitantly, nutrient starvation also promotes activation of TFEB/TFE3 factors and enhances ER-phagy in chondrocytes.

Results

FGF signaling activates TFEB/TFE3 through the insulin/PI3K signaling pathway inhibition

TFEB and TFE3 activity is negatively regulated by phosphorylation on specific serine residues by nutrient and growth factor responsive kinases [89], such as mTORC1 and AKT. When phosphorylated, TFEB and TFE3 nuclear translocation is inhibited, hence they are inactive; on the contrary, the inhibition of these kinases, such as during starvation, promote TFEB and TFE3 dephosphorylation, nuclear translocation and activation of target genes [89]. To characterize the mechanism by which FGF signaling activated TFEB/TFE3 in chondrocytes we performed phospho-proteomics analysis that allowed us to quantify the dynamic response of approximately 20,000 phospho-sites upon FGF stimulation. We observed that insulin and PI3K-signaling scored as the most significantly inhibited upon FGF18 stimulation in chondrocytes. By mapping phospho-proteome and proteome profiles on a literature-curated insulin/IGF signaling network, we identified IRS1, the adaptor protein that transmits signals from the insulin/IGF receptors [90], as the most down-regulated protein by FGF18 treatment in chondrocytes (**Figure 19**).
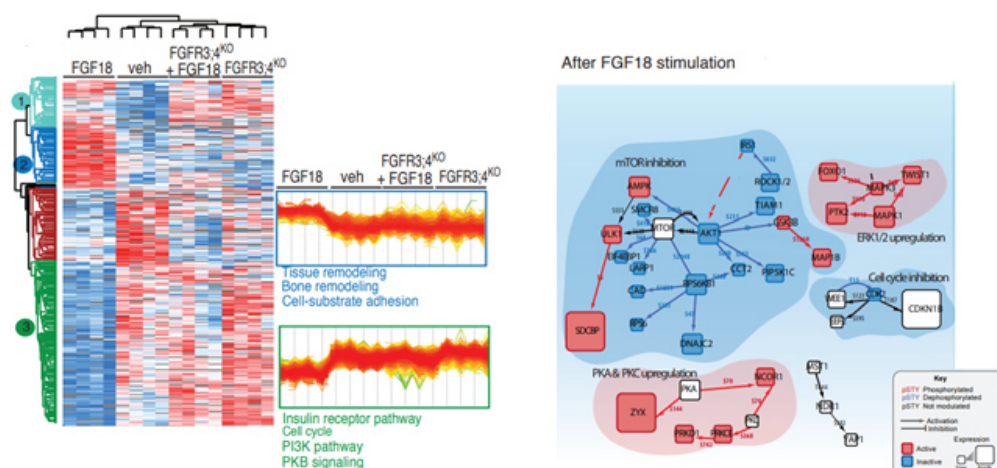

Figure 19. FGF signaling inhibits the insulin/PI3K signaling through down-regulation of IRS1.

(**Left**) MS-phospho-proteomics analysis of RCS chondrocytes with indicated genotypes treated with vehicle (5% ABS) and FGF18 (50 ng/mL) for 12 hours, showing biological

processes regulated by FGF signaling (in blue: upregulated, in green: down-regulated). N=4 biological replicates were analyzed. FDR<0.05.

(**Right**) Proteomic signaling network modulated by FGF18 in chondrocytes. Red=activating phosphorylation; blue= inhibitory phosphorylation. Cubes dimensions are relative to level of protein regulation.

Consistently, western blot analysis demonstrated that the activities of AKT and mTORC1 kinases, downstream of the PI3K signaling, were strongly reduced following FGF18 treatment (**Figure 20**). IRS1 down-regulation upon FGF stimulation was the consequence of its enhanced degradation, since it was prevented by treatment of RCS with the proteasome inhibitor MG132. The proteasomal degradation of IRS1 is triggered by phosphorylation mediated by different kinases, such as JNK1/2, mTORC1 or S6K21 [90]. FGF18 induced JNK1/2 activity, as demonstrated by phosphorylation of c-JUN, and pharmacological inhibition of JNK1/2 kinases blocked IRS1 degradation in FGF18 treated chondrocytes. Notably, IRS1 overexpression as well as JNK1/2 inhibition rescued mTORC1 and AKT signaling inhibition (**Figure 20**). mTORC1 and AKT phosphorylate TFEB and inhibit its nuclear translocation, thus we tested whether JNK-mediated IRS1 degradation induced TFEB and TFE3 nuclear translocation. Consistent with this hypothesis, TFEB/TFE3 dephosphorylation and nuclear translocation following FGF18 stimulation were inhibited in chondrocytes overexpressing IRS1, treated with JNK1-inhibitor (**Figure 20** and **Figure 21**). Collectively, these data suggest that FGF18 induces TFEB and TFE3- mediated lysosome biogenesis and ER-phagy via JNK-mediated IRS1 degradation and PI3K signaling inhibition.
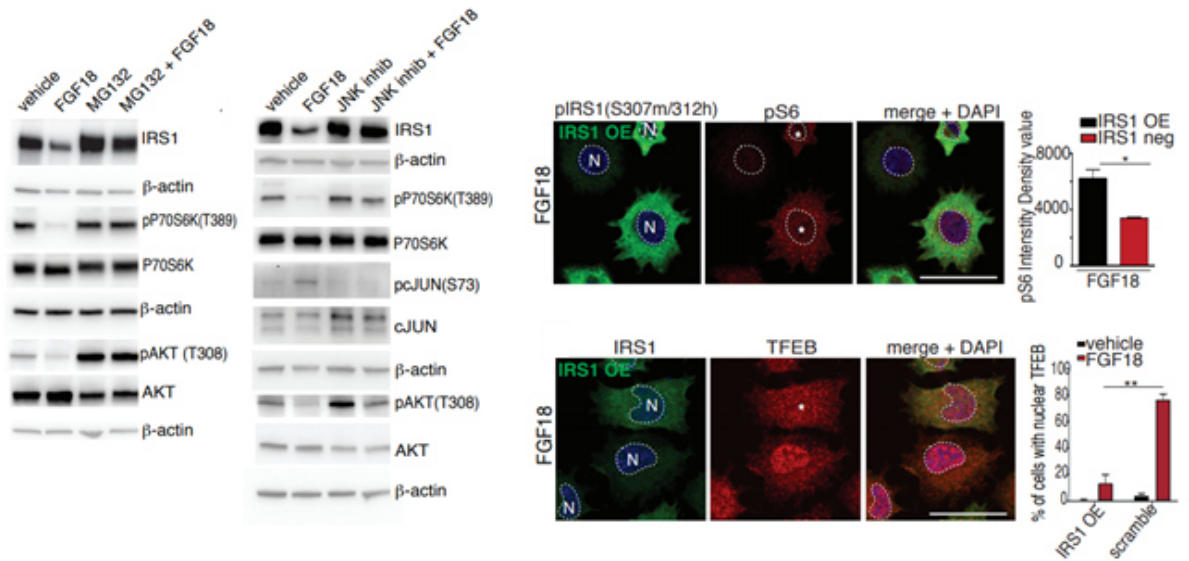
Figure 20. FGF signaling activates TFEB/TFE3 through the insulin/PI3K signaling pathway inhibition.

(**Left**) Western blot analysis of IRS1, pP70S6K (T389), P70S6K, pAKT (T308) and AKT in RCS chondrocytes treated with vehicle (5% ABS) and FGF18 (50 ng/mL) for 12h. MG132 was used at 10 µM for 6h to inhibit proteasome activity. β-actin was used as loading control. Blots are representative of N=3 independent experiments.

(**Centre**) Western blot analysis of IRS1, pP70S6K (T389), P70S6K, pAKT (T308), AKT, pcJUN (S73) and cJUN proteins in RCS chondrocytes treated with vehicle (5% ABS) and FGF18 (50 ng/mL) for 12h. JNK inhibitor was used at 50 µM for 12h to inhibit kinase activity. β-actin was used as loading control. Blots are representative of N=3 independent experiments.

(**Right**) Co-immunofluorescence of pIRS1 (S307 mouse/S312 human, in green) and pS6 (S240/S242, in red) ribosomal protein in IRS1-overexpressing RCS chondrocytes treated with FGF18 (50 ng/mL) for 12h. Asterisks indicate IRS1-overexpressing cells. Nuclei (N) were stained with DAPI (blue). Scale bar 15 µm. Quantification analysis of pS6 ribosomal protein fluorescence intensity in IRS1-overexpressing vs non expressing RCS chondrocytes. Mean +/- standard error of the mean (sem) of N=3 biological replicates. n=35 cells analyzed. Student's paired T-test *$p < 0.05$. Co-immunofluorescence of TFEB (red) and IRS1 (green) in IRS1-overexpressing RCS chondrocytes treated with FGF18 (50 ng/mL) for 12h. Asterisks indicate IRS1-overexpressing cells. Nuclei (N) were stained with DAPI (blue). Mean +/- standard error of the mean (sem) of N=3 biological replicates. Scale bar 15 µm. n= 124 cells analyzed; Student's un-paired T-test **$p < 0.005$.
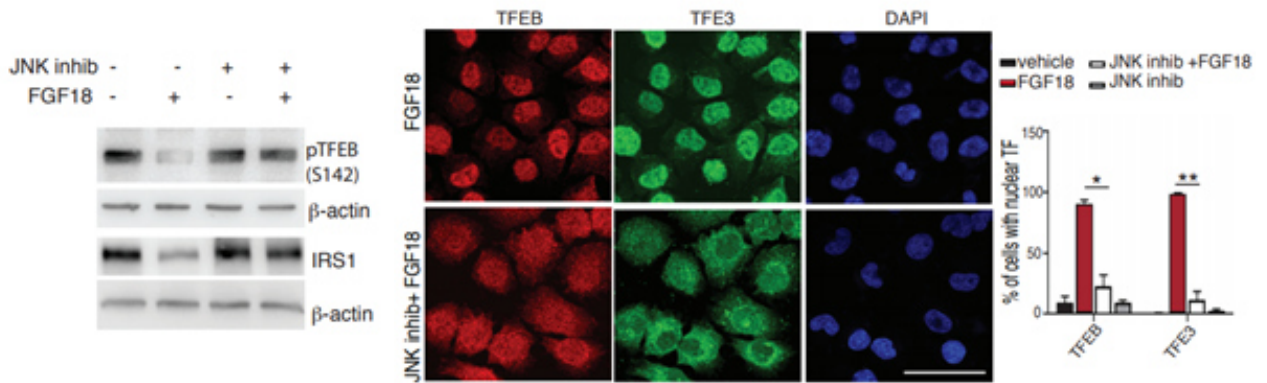
Figure 21. FGF signaling activates TFEB/TFE3 through JNK-mediated degradation of IRS1.

(**Left**) Western blot analysis of IRS1 and phospho-TFEB (S142) in RCS chondrocytes treated with vehicle (5% ABS) and FGF18 (50 ng/mL) for 12h. JNK inhibitor was used at 50 μM for 12h to inhibit kinase activity. β-actin was used as loading control. Representative images of N=3 independent experiments.

(**Right**) Subcellular localization analysis of TFEB (red) and TFE3 (green) in RCS chondrocytes treated with FGF18 (50 ng/mL) for 12h. JNK inhibitor was used at 50 μM for 12h. Nuclei were stained with DAPI (blue). Quantification analysis showed % of cells with nuclear TFEB and TFE3 in RCS chondrocytes with indicated treatments. Mean +/- standard error of the mean (sem) of N=3 biological replicates. Scale bar 15 μm. n= 126 cells (control), 126 cells (FGF18), 95 cells (JNK Inhibitor), 163 cells (JNK Inhibitor + FGF18). Student's paired T-test *$p < 0.05$; **$p < 0.005$.

Nutrient starvation promotes mTORC1 inhibition and TFEB nuclear translocation

Next, we asked whether the TFEB/TFE3 axis was also activated during nutrient and growth factor starvation. Starvation with HBSS media induced mTORC1 inhibition, along with TFEB nuclear translocation and dephosphorylation (**Figure 22**), further promoting ER-phagy via Fam134b transcriptional induction (data not shown). These data overall demonstrate that ER-phagy is a process transcriptionally regulated by TFEB and TFE3 nuclear factors via direct induction of the FAM134B protein, by both starvation and stimulation of the FGF signaling pathway in chondrocytes.
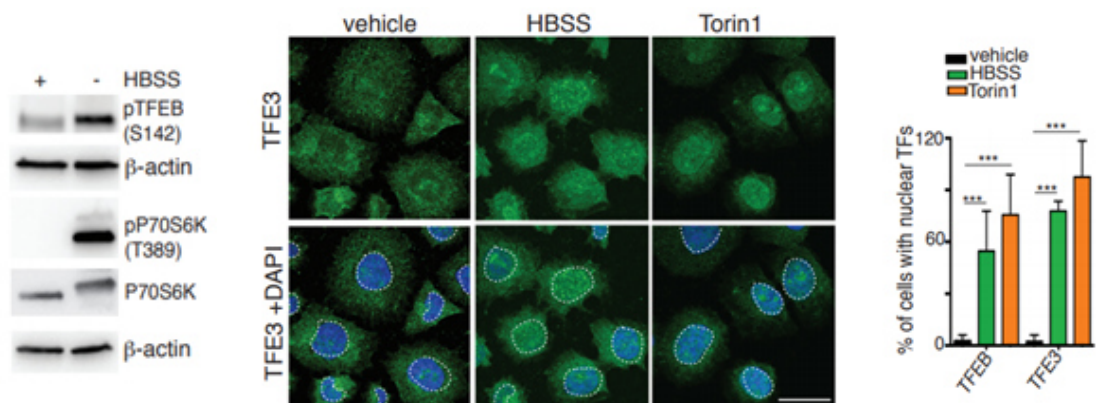
Figure 22. TFEB/TFE3 axis is activated during starvation.

(**Left**) Western blot analysis of pospho-P70S6K (T389), P70S6K, and phospho-TFEB (S142) in RCS chondrocytes cultured in complete medium or HBSS for 12h. β-actin was used as loading control.

(**Right**) Subcellular localization analysis of TFE3 (green) in RCS chondrocytes starved with HBSS for 8h. Torin1 was used at 1μM for 2h as positive control. Nuclei were stained with DAPI (blue). Quantification analysis showed % of cells with nuclear TFEB and TFE3 in RCS chondrocytes with indicated treatments. Mean +/- standard error of the mean (sem) of N=3 biological replicates/treatment. Scale bar 10 μm. n= 62 cells (control), 83 cells (HBSS), 47 cells (Torin1). Analysis of variance one way (ANOVA) p<0.0001; Sidak 's multiple comparison test ***p<0.0005.

Fam134b-Morpholino shows impaired bone mineralization

Knock-down of Fam134b with a specific morpholino (MO) directed against the second splice donor site in the Medaka fish (Oryzias latipes, ol) led to a shorter body length and head size with structural abnormalities mainly restricted to bones. Notably, both size and mineralization of craniofacial elements that form through endochondral ossification (ethmoid plate, palatoquadrate, ceratohyal, paired prootics and fifth ceratobranchial) were severely reduced compared with controls (**Figure 23**). These observations suggest that Fam134B-mediated ER-phagy plays a physiological role during endochondral ossification.
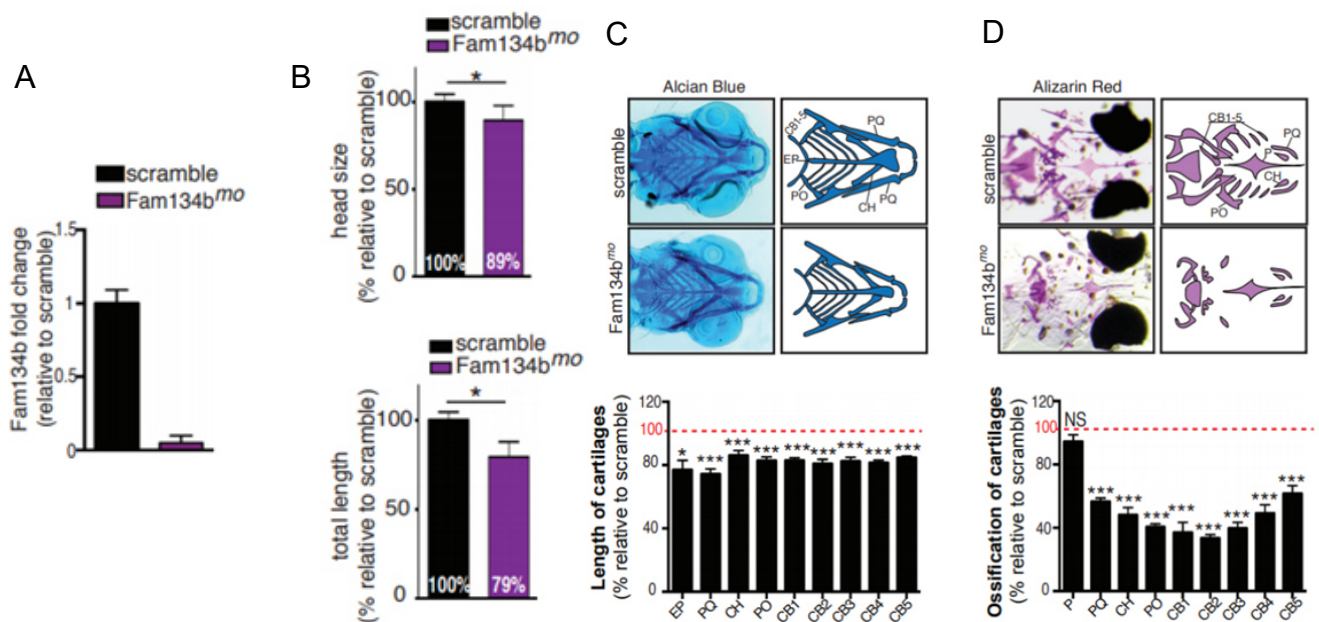
Figure 23. FAM134B knockdown in Medaka embryos is associated to defective endochondral ossification.

(**A**) qRT-PCR analysis of Fam134b gene in medaka fish with indicated genotypes. Fold change values are relative to scramble fish and normalized to Hprt gene. Mean +/- standard error of the mean (sem) of N=3 biological replicates. (**B**) Quantification of total length and head size of medaka fish model of Fam134b-morpholino expressed as % relative to the scramble. Mean +/- standard error of the mean (sem) of n=9 fish/genotype. Student unpaired T-Test *p<0.05. (**C**) Alcian blue (cartilage) staining of scramble and Fam134b-morpholino medaka fish. Graph shows quantification of Ethmoid plate (EP), Palatoquadrate (PQ),

Ceratohyal (CH), Paired Prootics (PO), Ceretobranchials 1 to 5 (CB1 to CB5) cartilage length in Fam134b-morpholino and scramble. Values were expressed as % relative to the scramble (100% red dotted line). Mean +/- standard error of the mean (sem) of n=9 fish/genotype. Student unpaired T-Test*$p<0.05$; ***$p<0.0005$. (**D**) Alizarin Red S (bone) staining of scramble and Fam134b morpholino medaka fish. Graph shows quantification of Parasphenoid (P), Palatoquadrate (PQ), Ceratohyal (CH), Paired Prootics (PO), Ceretobranchials 1 to 5 (CB1 to CB5) mineralization in Fam134b-morpholino. Values were expressed as % relative to the scramble (100% red dotted line). Mean +/- standard error of the mean (sem) of n=8 fish/genotype. Student unpaired T-Test ***$p<0.0005$; NS not significant.

Discussion

This study has identified a novel signaling pathway that allows ER-phagy responding to both metabolic and developmental cues. This work has revealed that the nutrient-regulated signaling network downstream TFEB and TFE3 transcription factors respond to extracellular cues, such as starvation and FGF signaling. Specifically, TFEB and TFE3 induce expression of lysosomal and autophagy genes and of the ER-phagy receptor FAM134B, hence they exert a global enhancement of ER-phagy, from substrate sequestration to autophagic cargo delivery and lysosomal degradation.

TFEB and TFE3 nuclear factors are part of the MiTF/TFE transcription factor family, participating to the biogenesis and co-operative functions of AVs and lysosomes, by binding of a sequence in the promoter of lysosomal genes, called as Coordinated Lysosomal Expression and Regulation (CLEAR) network [91]. The activity of TFEB and TFE3 factors is mostly regulated by phosphorylation on different serine residues operated by different kinases, such as mTORC1 and AKT [89]. mTORC1 (the Mammalian Target of Rapamycin Complex 1) is a serine/threonine phosphatidylinositol-3-kinase-related kinase (PI3K) and it covers a central role in the regulation of cellular metabolism and organismal growth. In this work, we have identified the mechanism downstream the FGF signaling pathways in

chondrocytes. Specifically, we have identified that the FGF signaling induces an inhibition of the PI3K signaling via a JNK-mediated degradation of IRS1, a key upstream protein in the PI3K signaling pathway [90].

The process of ER-phagy in chondrocytes overall participates to cell differentiation and tissue development. In fact, the lack of Fam134b in Medaka fish shows impaired endochondral ossification evidencing how this pathway is likely to play physiologically relevant roles in chondrocytes. The observation that starvation and FGF signaling activates ER-phagy through same effectors suggests that ER-phagy may participate to regulation of energy metabolism in chondrocytes, which reside in a tissue environment characterized by scarcity of nutrients, such as the growth plate [92]. During endochondral ossification FGF signaling controls chondrocyte hypertrophic differentiation [93, 94], a process that might require energy from the degradation of intracellular sources. The discovery of the cellular mechanisms governing ER-phagy can be of therapeutic relevance. Thus, the identification of the mechanisms controlling ER-phagy might be exploited for the treatment of protein conformational diseases.

Material and Methods

Cell Culture, transfections and Plasmids

RCS were cultured as previously shown. In FGF18 experiments, cells were cultured in DMEM supplemented with 5% Adult Bovine Serum (ABS from Bio-Techne). In starvation experiment, RCS chondrocytes were cultured in HBSS medium (from Euroclone). For transfection experiments: cells were transfected with Lipofectamine LTX and Plus reagent (Invitrogen) following reverse transfection protocol according to manufacturer's instructions. Plasmids: human-IRS1- WT plasmid was from Addgene. Chemicals: FGFs ligands (Peprotech) were used at 50ng/ml overnight. c-Jun N-Terminal kinase (JNK) inhibitor (SP600125, Sigma-Aldrich, Milan, Italy) was used at 50 µM for 12h. Torin1 (Cell Signaling) was used at 1 µM for 2h. Proteasomal inhibitor (MG132, Sigma-Aldrich, Milan, Italy) was used at 10 µM for 6h.

Immunofluorescence

RCS chondrocytes were fixed for 15 min in 4% PFA in PBS and permeabilized for 20 min in blocking buffer (0.05% (w/v) saponin, 0.5% (w/v) BSA, 50 mM NH4Cl and 0.02% NaN3 in PBS). Cells were incubated in humid chamber for 1 h at room 22 temperature with primary antibodies (p-IRS1 Merck 05-1087 1:100; IRS1 Cell Signaling Technology 2390 1:100; p-S6 Ribosomal protein Cell Signaling Technology 5364S 1:100), washed three times in PBS, incubated for 1 h at room temperature with the secondary (Alexa fluor-labeled 1:400) antibodies, washed again three times in PBS, incubated for 20 min with 1µg/ml Hoechst 33342 and finally mounted in Mowiol. All confocal experiments were acquired using slice thickness of 0.5 µm using the LSM 880 confocal microscope equipped with a 63× 1.4 numerical aperture oil objective. For TFEB and TFE3 immunofluorescence: RCS chondrocytes were fixed for 15 min in 4% PFA in PBS and permeabilized for 30 min in 0.02% Triton X-100 in PBS. Cells were incubated in humid chamber for 1h in Blocking

Buffer (0.1% Triton X100, 10% goat serum in PBS) and then with primary antibodies overnight at 4°C (TFEB MyBioSource MBS120432 1:50; TFE3 Sigma-Aldrich HPA023881 1:200) diluted in 0.1% Triton X-100, 5% goat serum in PBS. Alexa-fluor conjugated secondary antibodies (1:400) were incubated for 1h at room temperature in 0.1% Triton X-100, 1% goat serum in PBS. Nuclei were stained with DAPI 1:1000 in PBS for 20 min at room temperature. Cells were washed with PBS, once in MilliQ water and mounted with Mowiol. All images were captured using LSM 880 confocal microscope equipped with a 63× 1.4 numerical aperture oil objective. All the quantifications were performed used ImageJ plugins.

Western Blotting

RCS chondrocytes lysates were prepared as previously shown. Protein extracts, separated by SDS-PAGE and transferred onto PVDF, were probed with primary antibodies overnight against IRS1 (Cell Signaling Technology 2390 1:1000), phospho-P70S6K (Cell Signaling Technology 9234S 1:1000), P70S6K (Cell Signaling Technology 9202S 1:1000), phospho-AKT (Cell Signaling Technology 4056 (T308) - 4060 (S473) 1:1000), AKT (Cell Signaling Technology 9272 1:1000), phospho-cJUN (Cell Signaling Technology 2361S 1:1000), cJUN (Cell Signaling Technology 9165 1:1000), b-actin (Novus Biologicals 24 NB600-501 1:5000), TFEB (Bethyl Laboratories A303-673A 1:1000), TFE3 (Sigma-Aldrich HPA023881 1:1000), b-tubulin (Sigma T8660 1:10000), phospho-TFEB S142 (ABE1971 EMD Millipore 1:10000). Proteins of interest were detected with HRP conjugated goat anti-mouse or anti-rabbit IgG antibody (1: 2000, Vector Laboratories) and visualized with the ECL Star Enhanced Chemiluminescent Substrate (Euroclone) according to the manufacturer's protocol. The Western blotting images were acquired using the Chemidoc-lt imaging system (UVP).

qRT-PCR in Medaka Fishes

Medaka fishes were pooled for RNA extraction using RNeasy Mini Kit (Cat No./ID: 74106 (250), Qiagen) according to the manufacturer's protocol. 1 µg of total RNA was used for reverse transcription using QuantiTect Reverse Transcription Kit (Qiagen) according to manufacturer's instructions. qRT-PCR was performed in triplicate using Light Cycler 480 SYBER Green I Master (Roche) and analyzed by Light Cycler 480 (Roche). The Ct values were normalized to Hprt gene and the expression of each gene was represented as $2^{\wedge}(-ddCt)$ relative to control. Primers used were: Fam134b Fw5'-TCACTGCTGGAAGAAACCTG-3' Fam134b Rev5' –ATCATGAGACGAAACCAGGG-3'.

Medaka stocks

The Cab-strain of wild type medaka fish (Oryzias latipes) was maintained following standard conditions (i.e., 12 h/12 h dark/light conditions at 27 °C). Embryos were staged according to [83]. All studies on fish were conducted in strict accordance with the Institutional Guidelines for animal research and approved by the Italian Ministry of Health; Department of Public Health, Animal Health, Nutrition, and Food Safety in accordance to the law on animal experimentation (D.Lgs. 26/2014). Furthermore, all animal treatments were reviewed and approved in advance by the Ethics Committee at the TIGEM Institute, (Pozzuoli, NA), Italy.

Fam134b morpholino injections

The available medaka olFam134b (DK136186) genomic sequences were retrieved from public databases (http://genome.ucsc.edu/) from human FAM134b (NM_001034850) transcript. A morpholino (Mo; Gene Tools LLC, Oregon, USA) was designed against the splicing acceptor of exon 2 (MO-Fam134b: 5′- GTCGATGATCTCCCAACTGAAGACA-3′) of the medaka orthologous of the NEK10 gene. The specificity and inhibitory efficiencies

of morpholino was determined as previously described [95]. MO-Fam134b was injected at 0.015 mM concentration into one blastomere at the one/two-cell stage. Off-target effects of the morpholino injections were excluded by repeated experiments with control morpholino or by co-injection with a p53 morpholino as previously described [96].

Cartilage and bones staining

Staining for cartilage (Alcian Blue) and bone (Alizarin Red) in fixed embryos was performed according to standard Medaka skeleton phenotyping protocols (https://shigen.nig.ac.jp/medaka/medakabook/index.php). Pictures were taken using the DM6000 microscopy (Leica Microsystems, Wetzlar, Germany). Measurement of both cartilage and bone length was performed using ImageJ.

References

1. Mizushima, N. (2011) Autophagy in protein and organelle turnover, *Cold Spring Harbor symposia on quantitative biology.* **76**, 397-402.

2. Stolz, A., Ernst, A. & Dikic, I. (2014) Cargo recognition and trafficking in selective autophagy, *Nature cell biology.* **16**, 495-501.

3. Rogov, V. V., Stolz, A., Ravichandran, A. C., Rios-Szwed, D. O., Suzuki, H., Kniss, A., Lohr, F., Wakatsuki, S., Dotsch, V., Dikic, I., Dobson, R. C. & McEwan, D. G. (2018) Structural and functional analysis of the GABARAP interaction motif (GIM), *EMBO reports.* **19**.

4. Rogov, V., Dotsch, V., Johansen, T. & Kirkin, V. (2014) Interactions between autophagy receptors and ubiquitin-like proteins form the molecular basis for selective autophagy, *Molecular cell.* **53**, 167-78.

5. Schwarz, D. S. & Blower, M. D. (2016) The endoplasmic reticulum: structure, function and response to cellular signaling, *Cellular and molecular life sciences : CMLS.* **73**, 79-94.

6. Braakman, I. & Hebert, D. N. (2013) Protein folding in the endoplasmic reticulum, *Cold Spring Harbor perspectives in biology.* **5**, a013201.

7. Gomez-Navarro, N. & Miller, E. (2016) Protein sorting at the ER-Golgi interface, *The Journal of cell biology.* **215**, 769-778.

8. Muniz, M., Morsomme, P. & Riezman, H. (2001) Protein sorting upon exit from the endoplasmic reticulum, *Cell.* **104**, 313-20.

9. Bravo, R., Parra, V., Gatica, D., Rodriguez, A. E., Torrealba, N., Paredes, F., Wang, Z. V., Zorzano, A., Hill, J. A., Jaimovich, E., Quest, A. F. & Lavandero, S. (2013) Endoplasmic reticulum and the unfolded protein response: dynamics and metabolic integration, *International review of cell and molecular biology.* **301**, 215-90.

10. Fulda, S., Gorman, A. M., Hori, O. & Samali, A. (2010) Cellular stress responses: cell survival and cell death, *International journal of cell biology.* **2010**, 214074.

11. Drummond, D. A. & Wilke, C. O. (2009) The evolutionary consequences of erroneous protein synthesis, *Nature reviews Genetics.* **10**, 715-24.

12. Xu, C., Bailly-Maitre, B. & Reed, J. C. (2005) Endoplasmic reticulum stress: cell life and death decisions, *The Journal of clinical investigation.* **115**, 2656-64.

13. Dobson, C. M. (2002) Getting out of shape, *Nature.* **418**, 729-30.

14. Ogen-Shtern, N., Ben David, T. & Lederkremer, G. Z. (2016) Protein aggregation and ER stress, *Brain research.* **1648**, 658-666.

15. Kikis, E. A., Gidalevitz, T. & Morimoto, R. I. (2010) Protein homeostasis in models of aging and age-related conformational disease, *Advances in experimental medicine and biology.* **694**, 138-59.

16. Cuanalo-Contreras, K., Mukherjee, A. & Soto, C. (2013) Role of protein misfolding and proteostasis deficiency in protein misfolding diseases and aging, *International journal of cell biology.* **2013**, 638083.

17. Lopez-Otin, C., Blasco, M. A., Partridge, L., Serrano, M. & Kroemer, G. (2013) The hallmarks of aging, *Cell.* **153**, 1194-217.

18. Chiramel, A. I., Dougherty, J. D., Nair, V., Robertson, S. J. & Best, S. M. (2016) FAM134B, the Selective Autophagy Receptor for Endoplasmic Reticulum Turnover, Inhibits Replication of Ebola Virus Strains Makona and Mayinga, *The Journal of infectious diseases.* **214**, S319-S325.

19. Lennemann, N. J. & Coyne, C. B. (2017) Dengue and Zika viruses subvert reticulophagy by NS2B3-mediated cleavage of FAM134B, *Autophagy.* **13**, 322-332.

20. Moretti, J., Roy, S., Bozec, D., Martinez, J., Chapman, J. R., Ueberheide, B., Lamming, D. W., Chen, Z. J., Horng, T., Yeretssian, G., Green, D. R. & Blander, J. M. (2017) STING Senses Microbial Viability to Orchestrate Stress-Mediated Autophagy of the Endoplasmic Reticulum, *Cell.* **171**, 809-823 e13.

21. Ishida, Y., Yamamoto, A., Kitamura, A., Lamande, S. R., Yoshimori, T., Bateman, J. F., Kubota, H. & Nagata, K. (2009) Autophagic elimination of misfolded procollagen aggregates in the endoplasmic reticulum as a means of cell protection, *Molecular biology of the cell.* **20**, 2744-54.

22. Fujita, E., Kouroku, Y., Isoai, A., Kumagai, H., Misutani, A., Matsuda, C., Hayashi, Y. K. & Momoi, T. (2007) Two endoplasmic reticulum-associated degradation (ERAD) systems for the novel variant of the mutant dysferlin: ubiquitin/proteasome ERAD(I) and autophagy/lysosome ERAD(II), *Human molecular genetics.* **16**, 618-29.

23. Ellgaard, L. & Helenius, A. (2003) Quality control in the endoplasmic reticulum, *Nature reviews Molecular cell biology.* **4**, 181-91.

24. Preston, G. M. & Brodsky, J. L. (2017) The evolving role of ubiquitin modification in endoplasmic reticulum-associated degradation, *The Biochemical journal.* **474**, 445-469.

25. Ruggiano, A., Foresti, O. & Carvalho, P. (2014) Quality control: ER-associated degradation: protein quality control and beyond, *The Journal of cell biology.* **204**, 869-79.

26. Settembre, C., Fraldi, A., Medina, D. L. & Ballabio, A. (2013) Signals from the lysosome: a control centre for cellular clearance and energy metabolism, *Nature reviews Molecular cell biology.* **14**, 283-96.

27. Ishida, Y. & Nagata, K. (2009) Autophagy eliminates a specific species of misfolded procollagen and plays a protective role in cell survival against ER stress, *Autophagy.* **5**, 1217-9.

28. Hidvegi, T., Ewing, M., Hale, P., Dippold, C., Beckett, C., Kemp, C., Maurice, N., Mukherjee, A., Goldbach, C., Watkins, S., Michalopoulos, G. & Perlmutter, D. H. (2010) An autophagy-enhancing drug promotes degradation of mutant alpha1-antitrypsin Z and reduces hepatic fibrosis, *Science (New York, NY).* **329**, 229-32.

29. Noda, T. & Farquhar, M. G. (1992) A non-autophagic pathway for diversion of ER secretory proteins to lysosomes, *The Journal of cell biology.* **119**, 85-97.

30. Houck, S. A., Ren, H. Y., Madden, V. J., Bonner, J. N., Conlin, M. P., Janovick, J. A., Conn, P. M. & Cyr, D. M. (2014) Quality control autophagy degrades soluble ERAD-resistant conformers of the misfolded membrane protein GnRHR, *Molecular cell.* **54**, 166-179.

31. Smith, M. D., Harley, M. E., Kemp, A. J., Wills, J., Lee, M., Arends, M., von Kriegsheim, A., Behrends, C. & Wilkinson, S. (2018) CCPG1 Is a Non-canonical Autophagy Cargo Receptor Essential for ER-Phagy and Pancreatic ER Proteostasis, *Developmental cell.* **44**, 217-232 e11.

32. Forrester, A., De Leonibus, C., Grumati, P., Fasana, E., Piemontese, M., Staiano, L., Fregno, I., Raimondi, A., Marazza, A., Bruno, G., Iavazzo, M., Intartaglia, D., Seczynska, M., van Anken, E., Conte, I., De Matteis, M. A., Dikic, I., Molinari, M. & Settembre, C. (2019) A selective ER-phagy exerts procollagen quality control via a Calnexin-FAM134B complex, *The EMBO journal.* **38**.

33. Omari, S., Makareeva, E., Roberts-Pilgrim, A., Mirigian, L., Jarnik, M., Ott, C., Lippincott-Schwartz, J. & Leikin, S. (2018) Noncanonical autophagy at ER exit sites regulates procollagen turnover, *Proceedings of the National Academy of Sciences of the United States of America.* **115**, E10099-E10108.

34. Fregno, I., Fasana, E., Bergmann, T. J., Raimondi, A., Loi, M., Solda, T., Galli, C., D'Antuono, R., Morone, D., Danieli, A., Paganetti, P., van Anken, E. & Molinari, M. (2018) ER-to-lysosome-associated degradation of proteasome-resistant ATZ polymers occurs via receptor-mediated vesicular transport, *The EMBO journal.* **37**.

35. Klionsky, D. J. & Ohsumi, Y. (1999) Vacuolar import of proteins and organelles from the cytoplasm, *Annual review of cell and developmental biology.* **15**, 1-32.

36. Li, W. W., Li, J. & Bao, J. K. (2012) Microautophagy: lesser-known self-eating, *Cellular and molecular life sciences : CMLS.* **69**, 1125-36.

37. Bernales, S., McDonald, K. L. & Walter, P. (2006) Autophagy counterbalances endoplasmic reticulum expansion during the unfolded protein response, *PLoS biology.* **4**, e423.

38. Hamasaki, M., Noda, T., Baba, M. & Ohsumi, Y. (2005) Starvation triggers the delivery of the endoplasmic reticulum to the vacuole via autophagy in yeast, *Traffic.* **6**, 56-65.

39. Schuck, S., Gallagher, C. M. & Walter, P. (2014) ER-phagy mediates selective degradation of endoplasmic reticulum independently of the core autophagy machinery, *Journal of cell science.* **127**, 4078-88.

40. Mochida, K., Oikawa, Y., Kimura, Y., Kirisako, H., Hirano, H., Ohsumi, Y. & Nakatogawa, H. (2015) Receptor-mediated selective autophagy degrades the endoplasmic reticulum and the nucleus, *Nature.* **522**, 359-62.

41. Khaminets, A., Heinrich, T., Mari, M., Grumati, P., Huebner, A. K., Akutsu, M., Liebmann, L., Stolz, A., Nietzsche, S., Koch, N., Mauthe, M., Katona, I., Qualmann, B., Weis, J., Reggiori, F., Kurth, I., Hubner, C. A. & Dikic, I. (2015) Regulation of endoplasmic reticulum turnover by selective autophagy, *Nature.* **522**, 354-8.

42. English, A. R. & Voeltz, G. K. (2013) Endoplasmic reticulum structure and interconnections with other organelles, *Cold Spring Harbor perspectives in biology.* **5**, a013227.

43. Shemesh, T., Klemm, R. W., Romano, F. B., Wang, S., Vaughan, J., Zhuang, X., Tukachinsky, H., Kozlov, M. M. & Rapoport, T. A. (2014) A model for the generation and interconversion of ER morphologies, *Proceedings of the National Academy of Sciences of the United States of America.* **111**, E5243-51.

44. Nixon-Abell, J., Obara, C. J., Weigel, A. V., Li, D., Legant, W. R., Xu, C. S., Pasolli, H. A., Harvey, K., Hess, H. F., Betzig, E., Blackstone, C. & Lippincott-Schwartz, J. (2016) Increased spatiotemporal resolution reveals highly dynamic dense tubular matrices in the peripheral ER, *Science (New York, NY).* **354**.

45. Fumagalli, F., Noack, J., Bergmann, T. J., Cebollero, E., Pisoni, G. B., Fasana, E., Fregno, I., Galli, C., Loi, M., Solda, T., D'Antuono, R., Raimondi, A., Jung, M., Melnyk, A., Schorr, S., Schreiber, A., Simonelli, L., Varani, L., Wilson-Zbinden, C., Zerbe, O., Hofmann, K., Peter, M., Quadroni, M., Zimmermann, R. & Molinari, M. (2016) Translocon component Sec62 acts in endoplasmic reticulum turnover during stress recovery, *Nature cell biology.* **18**, 1173-1184.

46. Grumati, P., Morozzi, G., Holper, S., Mari, M., Harwardt, M. I., Yan, R., Muller, S., Reggiori, F., Heilemann, M. & Dikic, I. (2017) Full length RTN3 regulates turnover of tubular endoplasmic reticulum via selective autophagy, *eLife.* **6**.

47. An, H., Ordureau, A., Paulo, J. A., Shoemaker, C. J., Denic, V. & Harper, J. W. (2019) TEX264 Is an Endoplasmic Reticulum-Resident ATG8-Interacting Protein Critical for ER Remodeling during Nutrient Stress, *Molecular cell*.

48. Chino, H., Hatta, T., Natsume, T. & Mizushima, N. (2019) Intrinsically Disordered Protein TEX264 Mediates ER-phagy, *Molecular cell*.

49. Chen, Q., Teng, J. & Chen, J. (2019) ATL3, a cargo receptor for reticulophagy, *Autophagy*, 1-2.

50. Chen, Q., Xiao, Y., Chai, P., Zheng, P., Teng, J. & Chen, J. (2019) ATL3 Is a Tubular ER-Phagy Receptor for GABARAP-Mediated Selective Autophagy, *Current biology : CB.* **29**, 846-855 e6.

51. Voeltz, G. K., Prinz, W. A., Shibata, Y., Rist, J. M. & Rapoport, T. A. (2006) A class of membrane proteins shaping the tubular endoplasmic reticulum, *Cell.* **124**, 573-86.

52. Hu, J., Shibata, Y., Zhu, P. P., Voss, C., Rismanchi, N., Prinz, W. A., Rapoport, T. A. & Blackstone, C. (2009) A class of dynamin-like GTPases involved in the generation of the tubular ER network, *Cell.* **138**, 549-61.

53. Chino, H., Hatta, T., Natsume, T. & Mizushima, N. (2019) Intrinsically Disordered Protein TEX264 Mediates ER-phagy, *Molecular cell.* **74**, 909-921 e6.

54. Pengo, N., Scolari, M., Oliva, L., Milan, E., Mainoldi, F., Raimondi, A., Fagioli, C., Merlini, A., Mariani, E., Pasqualetto, E., Orfanelli, U., Ponzoni, M., Sitia, R., Casola, S. & Cenci, S. (2013) Plasma cells require autophagy for sustainable immunoglobulin production, *Nature immunology.* **14**, 298-305.

55. Jia, W., Pua, H. H., Li, Q. J. & He, Y. W. (2011) Autophagy regulates endoplasmic reticulum homeostasis and calcium mobilization in T lymphocytes, *Journal of immunology (Baltimore, Md : 1950).* **186**, 1564-74.

56. Schultz, M. L., Krus, K. L., Kaushik, S., Dang, D., Chopra, R., Qi, L., Shakkottai, V. G., Cuervo, A. M. & Lieberman, A. P. (2018) Coordinate regulation of mutant NPC1 degradation by selective ER autophagy and MARCH6-dependent ERAD, *Nature communications.* **9**, 3671.

57. Cunningham, C. N., Williams, J. M., Knupp, J., Arunagiri, A., Arvan, P. & Tsai, B. (2019) Cells Deploy a Two-Pronged Strategy to Rectify Misfolded Proinsulin Aggregates, *Molecular cell.* **75**, 442-456 e4.

58. Bateman, J. F., Boot-Handford, R. P. & Lamande, S. R. (2009) Genetic diseases of connective tissues: cellular and extracellular effects of ECM mutations, *Nature reviews Genetics.* **10**, 173-83.

59. Malhotra, V. & Erlmann, P. (2015) The pathway of collagen secretion, *Annual review of cell and developmental biology.* **31**, 109-24.

60. Bienkowski, R. S., Curran, S. F. & Berg, R. A. (1986) Kinetics of intracellular degradation of newly synthesized collagen, *Biochemistry.* **25**, 2455-9.

61. Cinque, L., Forrester, A., Bartolomeo, R., Svelto, M., Venditti, R., Montefusco, S., Polishchuk, E., Nusco, E., Rossi, A., Medina, D. L., Polishchuk, R., De Matteis, M. A. & Settembre, C. (2015) FGF signalling regulates bone growth through autophagy, *Nature.* **528**, 272-5.

62. Bartolomeo, R., Cinque, L., De Leonibus, C., Forrester, A., Salzano, A. C., Monfregola, J., De Gennaro, E., Nusco, E., Azario, I., Lanzara, C., Serafini, M., Levine, B., Ballabio, A. & Settembre, C. (2017) mTORC1 hyperactivation arrests bone growth in lysosomal storage disorders by suppressing autophagy, *The Journal of clinical investigation.* **127**, 3717-3729.

63. Settembre, C., Cinque, L., Bartolomeo, R., Di Malta, C., De Leonibus, C. & Forrester, A. (2018) Defective collagen proteostasis and matrix formation in the pathogenesis of lysosomal storage disorders, *Matrix biology : journal of the International Society for Matrix Biology.* **71-72**, 283-293.

64. Oestreich, A. K., Garcia, M. R., Yao, X., Pfeiffer, F. M., Nobakhti, S., Shefelbine, S. J., Wang, Y., Brodeur, A. C. & Phillips, C. L. (2015) Characterization of the MPS I-H knock-in mouse reveals increased femoral biomechanical integrity with compromised material strength and altered bone geometry, *Molecular genetics and metabolism reports.* **5**, 3-11.

65. Yang, S. S., Chen, H., Williams, P., Cacciarelli, A., Misra, R. P. & Bernstein, J. (1980) Spondyloepiphyseal dysplasia congenita. A comparative study of chondrocytic inclusions, *Archives of pathology & laboratory medicine.* **104**, 208-11.

66. Murray, L. W., Bautista, J., James, P. L. & Rimoin, D. L. (1989) Type II collagen defects in the chondrodysplasias. I. Spondyloepiphyseal dysplasias, *American journal of human genetics.* **45**, 5-15.

67. Shoji-Kawata, S., Sumpter, R., Leveno, M., Campbell, G. R., Zou, Z., Kinch, L., Wilkins, A. D., Sun, Q., Pallauf, K., MacDuff, D., Huerta, C., Virgin, H. W., Helms, J. B., Eerland, R., Tooze, S. A., Xavier, R., Lenschow, D. J., Yamamoto, A., King, D., Lichtarge, O., Grishin, N. V., Spector, S. A., Kaloyanova, D. V. & Levine, B. (2013) Identification of a candidate therapeutic autophagy-inducing peptide, *Nature.* **494**, 201-6.

68. Suzuki, H., Osawa, T., Fujioka, Y. & Noda, N. N. (2017) Structural biology of the core autophagy machinery, *Current opinion in structural biology.* **43**, 10-17.

69. DiChiara, A. S., Taylor, R. J., Wong, M. Y., Doan, N. D., Rosario, A. M. & Shoulders, M. D. (2016) Mapping and Exploring the Collagen-I Proteostasis Network, *ACS chemical biology.* **11**, 1408-21.

70. Oliver, J. D., Roderick, H. L., Llewellyn, D. H. & High, S. (1999) ERp57 functions as a subunit of specific complexes formed with the ER lectins calreticulin and calnexin, *Molecular biology of the cell.* **10**, 2573-82.

71. Hebert, D. N., Foellmer, B. & Helenius, A. (1995) Glucose trimming and reglucosylation determine glycoprotein association with calnexin in the endoplasmic reticulum, *Cell.* **81**, 425-33.

72. Keller, S. H., Lindstrom, J. & Taylor, P. (1998) Inhibition of glucose trimming with castanospermine reduces calnexin association and promotes proteasome degradation of the alpha-subunit of the nicotinic acetylcholine receptor, *The Journal of biological chemistry.* **273**, 17064-72.

73. Hein, M. Y., Hubner, N. C., Poser, I., Cox, J., Nagaraj, N., Toyoda, Y., Gak, I. A., Weisswange, I., Mansfeld, J., Buchholz, F., Hyman, A. A. & Mann, M. (2015) A human interactome in three quantitative dimensions organized by stoichiometries and abundances, *Cell.* **163**, 712-23.

74. Williams, D. B. (2006) Beyond lectins: the calnexin/calreticulin chaperone system of the endoplasmic reticulum, *Journal of cell science.* **119**, 615-23.

75. Bhaskara, R. M., Grumati, P., Garcia-Pardo, J., Kalayil, S., Covarrubias-Pinto, A., Chen, W., Kudryashev, M., Dikic, I. & Hummer, G. (2019) Curvature induction and membrane remodeling by FAM134B reticulon homology domain assist selective ER-phagy, *Nature communications.* **10**, 2370.

76. Kurokawa, K. & Nakano, A. (2019) The ER exit sites are specialized ER zones for the transport of cargo proteins from the ER to the Golgi apparatus, *Journal of biochemistry.* **165**, 109-114.

77. Kraus, A., Groenendyk, J., Bedard, K., Baldwin, T. A., Krause, K. H., Dubois-Dauphin, M., Dyck, J., Rosenbaum, E. E., Korngut, L., Colley, N. J., Gosgnach, S., Zochodne, D., Todd, K., Agellon, L. B. & Michalak, M. (2010) Calnexin deficiency leads to dysmyelination, *The Journal of biological chemistry.* **285**, 18928-38.

78. Solda, T., Galli, C., Kaufman, R. J. & Molinari, M. (2007) Substrate-specific requirements for UGT1-dependent release from calnexin, *Molecular cell.* **27**, 238-49.

79. Solda, T., Garbi, N., Hammerling, G. J. & Molinari, M. (2006) Consequences of ERp57 deletion on oxidative folding of obligate and facultative clients of the calnexin cycle, *The Journal of biological chemistry.* **281**, 6219-26.

80. Molinari, M., Eriksson, K. K., Calanca, V., Galli, C., Cresswell, P., Michalak, M. & Helenius, A. (2004) Contrasting functions of calreticulin and calnexin in glycoprotein folding and ER quality control, *Molecular cell.* **13**, 125-35.

81. Venditti, R., Scanu, T., Santoro, M., Di Tullio, G., Spaar, A., Gaibisso, R., Beznoussenko, G. V., Mironov, A. A., Mironov, A., Jr., Zelante, L., Piemontese, M. R., Notarangelo, A., Malhotra, V., Vertel, B. M., Wilson, C. & De Matteis, M. A. (2012) Sedlin controls the ER export of procollagen by regulating the Sar1 cycle, *Science (New York, NY).* **337**, 1668-72.

82. Carrella, S., Barbato, S., D'Agostino, Y., Salierno, F. G., Manfredi, A., Banfi, S. & Conte, I. (2015) TGF-beta Controls miR-181/ERK Regulatory Network during Retinal Axon Specification and Growth, *PloS one.* **10**, e0144129.

83. Iwamatsu, T. (2004) Stages of normal development in the medaka Oryzias latipes, *Mechanisms of development.* **121**, 605-18.

84. Rappsilber, J., Ishihama, Y. & Mann, M. (2003) Stop and go extraction tips for matrix-assisted laser desorption/ionization, nanoelectrospray, and LC/MS sample pretreatment in proteomics, *Analytical chemistry.* **75**, 663-70.

85. Cox, J., Neuhauser, N., Michalski, A., Scheltema, R. A., Olsen, J. V. & Mann, M. (2011) Andromeda: a peptide search engine integrated into the MaxQuant environment, *Journal of proteome research.* **10**, 1794-805.

86. Tyanova, S., Temu, T., Sinitcyn, P., Carlson, A., Hein, M. Y., Geiger, T., Mann, M. & Cox, J. (2016) The Perseus computational platform for comprehensive analysis of (prote)omics data, *Nature methods.* **13**, 731-40.

87. Karsenty, G., Kronenberg, H. M. & Settembre, C. (2009) Genetic control of bone formation, *Annual review of cell and developmental biology.* **25**, 629-48.

88. Napolitano, G. & Ballabio, A. (2016) TFEB at a glance, *Journal of cell science.* **129**, 2475-81.

89. Puertollano, R., Ferguson, S. M., Brugarolas, J. & Ballabio, A. (2018) The complex relationship between TFEB transcription factor phosphorylation and subcellular localization, *The EMBO journal.* **37**.

90. Haeusler, R. A., McGraw, T. E. & Accili, D. (2018) Biochemical and cellular properties of insulin receptor signalling, *Nature reviews Molecular cell biology.* **19**, 31-44.

91. Sardiello, M., Palmieri, M., di Ronza, A., Medina, D. L., Valenza, M., Gennarino, V. A., Di Malta, C., Donaudy, F., Embrione, V., Polishchuk, R. S., Banfi, S., Parenti, G., Cattaneo, E. & Ballabio, A. (2009) A gene network regulating lysosomal biogenesis and function, *Science (New York, NY).* **325**, 473-7.

92. Yao, Q., Khan, M. P., Merceron, C., LaGory, E. L., Tata, Z., Mangiavini, L., Hu, J., Vemulapalli, K., Chandel, N. S., Giaccia, A. J. & Schipani, E. (2019) Suppressing Mitochondrial Respiration Is Critical for Hypoxia Tolerance in the Fetal Growth Plate, *Developmental cell.* **49**, 748-763 e7.

93. Liu, Z., Lavine, K. J., Hung, I. H. & Ornitz, D. M. (2007) FGF18 is required for early chondrocyte proliferation, hypertrophy and vascular invasion of the growth plate, *Developmental biology.* **302**, 80-91.

94. Dailey, L., Laplantine, E., Priore, R. & Basilico, C. (2003) A network of transcriptional and signaling events is activated by FGF to induce chondrocyte growth arrest and differentiation, *The Journal of cell biology.* **161**, 1053-66.

95. Conte, I., Carrella, S., Avellino, R., Karali, M., Marco-Ferreres, R., Bovolenta, P. & Banfi, S. (2010) miR-204 is required for lens and retinal development via Meis2 targeting, *Proceedings of the National Academy of Sciences of the United States of America.* **107**, 15491-6.

96. Eisen, J. S. & Smith, J. C. (2008) Controlling morpholino experiments: don't stop making antisense, *Development (Cambridge, England).* **135**, 1735-43.